Dual-specificity phosphatases 13 and 27 as key switches in muscle stem cell transition from proliferation to differentiation

Takuto Hayashi[1], Shunya Sadaki[1,2], Ryosuke Tsuji[1,2], Risa Okada[3], Sayaka Fuseya[1,4], Maho Kanai[1], Ayano Nakamura[1,5], Yui Okamura[1,5], Masafumi Muratani[6], Gu Wenchao[7], Takehito Sugasawa[8], Seiya Mizuno[9], Eiji Warabi[1], Takashi Kudo[1], Satoru Takahashi[1*], Ryo Fujita[10, 11*]

[1] Laboratory Animal Resource Center in Transborder Medical Research Center, and Department of Anatomy and Embryology, Institute of Medicine, University of Tsukuba, Ibaraki 305-8575, Japan

[2] Ph.D. Program in Humanics, School of Integrative and Global Majors, University of Tsukuba, Ibaraki 305-8575, Japan

[3] JEM Utilization Center, Human Spaceflight Technology Directorate, Japan Aerospace Exploration Agency (JAXA), Ibaraki 305-8505, Japan

[4] Cellular and Molecular Biotechnology Research Institute, National Institute of Advanced Industrial Science and Technology, Ibaraki 305-8565, Japan

[5] College of Medicine, School of Medicine and Health Sciences, University of Tsukuba, Ibaraki 305-8575, Japan

[6] Department of Genome Biology, Transborder Medical Research Center, Institute of Medicine, University of Tsukuba, Ibaraki 305-8575, Japan

[7] Department of Diagnostic and Interventional Radiology, Institute of Medicine, University of Tsukuba, Ibaraki 305-8575, Japan

[8] Laboratory of Clinical Examination and Sports Medicine, Department of Clinical Medicine, Institute of Medicine, University of Tsukuba, Ibaraki 305-8575, Japan

[9] Laboratory Animal Resource Center in Transborder Medical Research Center, and Department of Laboratory Animal Science, Institute of Medicine, University of Tsukuba, Ibaraki 305-8575, Japan.

[10] Division of Regenerative Medicine, Transborder Medical Research Center, Institute of Medicine, University of Tsukuba, Ibaraki 305-8575, Japan

[11] Lead contact

***Correspondence:**

Ryo Fujita, Ph.D.

Division of Regenerative Medicine, Transborder Medical Research Center, Institute of Medicine, University of Tsukuba, Ibaraki 305-8575, Japan.

E-mail: fujiryo@md.tsukuba.ac.jp

Satoru Takahashi, M.D., Ph.D.

Laboratory Animal Resource Center in Transborder Medical Research Center, and Department of Anatomy and Embryology, Institute of Medicine, University of Tsukuba, Ibaraki 305-8575, Japan
E-mail: satoruta@md.tsukuba.ac.jp

Summary

Muscle regeneration depends on muscle stem cell (MuSCs) activity. These cells are typically quiescent but become activated upon muscle injury, transitioning from proliferation to differentiation. Myogenic regulatory factors, including myoblast determination protein 1 (MyoD), regulate the fate transition of MuSCs. However, the role of MYOD in this process is not yet clear. Using previously established MyoD knock-in (MyoD-KI) mice, we revealed that MyoD targets dual-specificity phosphatase (Dusp) 13 and Dusp27. In *Dusp13*:*Dusp27* double knock-out (DKO) mice, the ability for muscle regeneration after injury was found to be reduced. Moreover, single-cell RNA sequencing of MyoD-high expressing MuSCs from MyoD-KI mice revealed that *Dusp13* and *Dusp27* are only expressed in specific populations within MyoD-high MuSCs, which also express *Myogenin*. Overexpressing *Dusp13* in MuSCs causes premature muscle differentiation. Thus, we propose a model where DUSP13 and DUSP27 contribute to the fate transition of MuSCs from proliferation to differentiation during myogenesis.

Keywords: Muscle stem cell, MyoD, Dual specificity phosphatase 13:27, Regeneration, Single-cell RNA-sequencing

INTRODUCTION

Skeletal muscle stem cells (MuSCs), also called satellite cells (Mauro, 1961), play a vital role in postnatal muscle development and the regeneration of skeletal muscles (Murphy et al., 2011). MuSCs are located near the myofibers beneath the basal lamina and exist in a quiescent state. However, in response to injury, they become activated, differentiate, and generate new myofibers (Collins et al., 2005; van Velthoven and Rando, 2019). Some of the progeny of the activated MuSCs undergo self-renewal to perpetually sustain the MuSC pool throughout a lifespan (Kuang et al., 2007; Sénéchal et al., 2022; Zammit et al., 2006).

The dynamics of MuSCs are intricately regulated by a series of myogenic regulatory factors (MRFs) that are sequentially expressed during myogenesis. Quiescent MuSCs express the paired homeodomain family of transcription factors PAX7 (Relaix et al., 2005; Seale et al., 2000). The MRFs, including MyoD, Myf5, myogenin, and MRF4, act as basic helix–loop–helix (bHLH) transcription factors that bind to E-box sites. While MYOD and MYF5 have overlapping functions as essential transcription factors for muscle lineage specification (Rudnicki et al., 1993; Yamamoto et al., 2018), MYOGENIN and MRF4 are indispensable for muscle differentiation (Kassar-Duchossoy et al., 2004; Nabeshima et al., 1993). Additionally, MRFs are induced in activated MuSCs during muscle regeneration in adult mice. Interestingly, quiescent MuSCs repress the translation of specific transcripts that keep them primed to rapidly activate the myogenic program in case of injury (Zismanov et al., 2016). MicroRNAs and RNA-binding proteins primarily mediate the repression of *Myf5* and *MyoD* transcripts (Crist et al., 2012; Fujita et al., 2017; Hausburg et al., 2015; de Morrée et al., 2017). Upon injury, the block on translation is lifted, leading to the rapid translation of *MyoD* and *Myf5*, initiating the myogenic program for regeneration.

MyoD knockout (KO) mice exhibited delayed myogenic differentiation and accelerated self-renewal ability in MuSCs. Furthermore, *MyoD* KO mice on an mdx background, a model for Duchenne muscular dystrophy, have a low survival rate (Megeney et al., 1996; Yablonka-Reuveni et al., 1999) . These reports suggest that MYOD plays a critical role in determining the fate of activated MuSCs by balancing self-renewal and differentiation during myogenesis. However, the specific mechanisms by which MYOD influences the fate of activated MuSCs remain unclear.

In a prior study, we created a MyoD knock-in (KI) reporter mouse line to recapitulate the expression levels of endogenous MyoD using tdTomato fluorescence (Fujita et al., 2023). This fluorescence allowed us to identify the state of MuSCs during myogenesis. We found that the MyoD-low population, characterized by low tdTomato fluorescence, consisted mostly of undifferentiated stem-like cells. On the other hand, the MyoD-high population, with high tdTomato fluorescence, showed features of committed and differentiating MuSC (Fujita et al., 2023). To investigate the molecular mechanisms governing the stemness and commitment/differentiation of MuSCs, we collected whole transcriptome data from MyoD-low MuSCs, MyoD-high MuSCs, and quiescent MuSCs isolated from Pax7$^{YFP/YFP}$

92 (Pax7-YFP) mice (Fujita et al., 2023; Kitajima and Ono, 2018). The establishment of MyoD-KI mice
93 and the availability of whole transcriptome data at different activation stages of MuSCs based on
94 MYOD levels provide a valuable platform for understanding the fate determination mediated by
95 MYOD.

96 The DUSP family comprises members of the protein tyrosine phosphatase superfamily involved in
97 the dephosphorylation of phosphotyrosine and phosphoserine/threonine residues (Alonso and Pulido,
98 2016; Denu and Dixon, 1995, 1998). They interact directly with MAPK effectors, including
99 extracellular signal-regulated kinases 1/2 (ERK1/2), leading to their dephosphorylation and
100 subsequent inactivation. Therefore, DUSPs play regulatory roles in cell growth, cell differentiation,
101 and apoptosis (Bermudez et al., 2010; Patterson et al., 2009; Tonks, 2006). The phosphatase domain
102 common to DUSPs is known as protein tyrosine phosphatases (PTP). DUSPs can be classified into
103 two subfamilies based on the presence or absence of the MAP kinase-binding (MKB) motif or the
104 kinase-interacting motif (KIM). The DUSPs with the KIM domain are classified as typical DUSPs,
105 whereas those lacking the KIM domain are classified as atypical DUSPs (Aoki et al., 2001; Huang
106 and Tan, 2012).

107 Interestingly, the functional regulation of substrates by DUSPs does not always require phosphatase
108 activity. DUSPs can control the function of MAPKs by sequestering them in the cytoplasm or nucleus.
109 It has also been observed that some DUSPs are catalytically inactive (Reiterer et al., 2020). For
110 example, DUSP27 lacks phosphatase activity due to the absence of a highly conserved cysteine residue
111 essential for enzyme activity (Fero et al., 2014). Nevertheless, the loss of *Dusp27* in zebrafish leads to
112 severe disorganization of the sarcomere structure, underscoring the significance of its
113 pseudophosphatase function in muscle development (Fero et al., 2014). Within skeletal muscles,
114 DUSP5 and DUSP6, classified as typical DUSPs, regulate muscle hypertrophy and myofiber types by
115 inhibiting ERK1/2 signaling (Boyer et al., 2019). However, our understanding of the function of
116 atypical DUSPs in skeletal muscle in mammals is limited.

117 In the present study, we used our MyoD-KI transcriptome and various datasets to identify *Dusp13*
118 as a direct target for MYOD. *Dusp13* is located on chromosome 10a22.2 and encodes two distinct
119 DUSPs, *Dusp13a* and *Dusp13b*. Although DUSP13a is predominantly expressed in murine skeletal
120 muscles (Chen et al., 2004), its specific roles in skeletal muscle remain unclear. Single KO of *Dusp13*
121 did not show any regenerative defects, but there was compensatory upregulation of *Dusp27* in skeletal
122 muscles lacking *Dusp13*. To further investigate, we generated a double KO (DKO) of *Dusp13* and
123 *Dusp27* and observed diminished muscle regeneration activity after acute muscle injury. Furthermore,
124 through single-cell RNA-seq (scRNA-seq) analysis, we found that the expressions of *Dusp13* and
125 *Dusp27* are limited to specific subsets of MyoD-high expressing MuSCs that also show the expression
126 of late myogenic markers. Based on these findings, we propose a model in which DUSP13 and

127 DUSP27 instigate the transition of MuSCs from an activated/proliferative state to a differentiation
128 state during regeneration.
129
130 **RESULTS**
131 ***Dusp13 is directly regulated by MyoD activity.***
132 We previously generated MyoD-KI mice that allow us to assess MYOD expression through tdTomato
133 fluorescence intensity (Fujita et al., 2023). To identify new regulators directly controlled by MYOD
134 activity, we utilized RNA-seq data from MyoD-low and MyoD-high expressing MuSCs from the
135 MyoD-KI mice, as well as freshly isolated quiescent MuSCs from $Pax7^{YFP/YFP}$ (Pax7-YFP) mice
136 (Figure 1A). Initially, we visualized the differentially expressed genes (FDR < 0.05) between the
137 MyoD-low and MyoD-high populations using a heatmap (Figure 1A). We found that 966 genes were
138 significantly upregulated as *MyoD* levels increased (MyoD-KI Cluster2). To further narrow down the
139 targets, we consulted a gene expression database of proliferating and differentiating MuSCs from
140 *MyoD* KO mice (Wang et al., 2022). We identified 1797 genes that were not upregulated in *MyoD* KO
141 mice (MKO Cluster2 in Figure 1B). Through a Venn diagram comparison, we combined 505 genes
142 from the MyoD-KI and MKO clusters. Additionally, when we included *MyoD* ChIP-seq data from
143 ChIP-Atlas, we found that 35 genes were enriched (Figure 1C) (Oki et al., 2018; Zou et al., 2022).
144 Finally, out of these 35 genes, six genes (*Ank1*, *Dmpk*, *Dusp13*, *Jsrp1*, *Rapsn*, and *Stac3*) were induced
145 by *MyoD* overexpression in mouse embryonic fibroblasts (MEFs) (Conerly et al., 2016) (Figure 1C
146 and 1D; Figure S1A and S1B). We also confirmed that *Dusp13* mRNA was predominantly enriched
147 in the quadriceps muscles compared to other tissues (Figure S2A).
148 Due to the modulation of *Dusp13* expression by *MyoD* (Figure 1E–1H), we assessed the E-box site
149 on *Dusp13*. We identified a highly conserved E-box site 150 bp upstream of the transcription initiation
150 site of *Dusp13*, according to the UCSC Genome Browser (Figure 1I). To determine if MYOD binds
151 to the E-box of *Dusp13*, we ligated the putative E-box site of *Dusp13* to a pGL4.10 vector to generate
152 a luciferase-*Dusp13*-E-box vector. We then co-transfected the plasmid with a *MyoD* expression vector
153 into the HEK293T cell line. The luciferase activity was significantly upregulated in the presence of
154 *MyoD* when the *Dusp13*-Ebox was present (Figure 1J). These results suggest that DUSP13 is a new
155 target of MYOD during myogenesis.
156
157 ***Single Dusp13 or Dusp27 KO mice exhibits no abnormality in muscle development or regeneration.***
158 To investigate the role of DUSP13 in skeletal muscle, we generated *Dusp13* KO mice using CRISPR-
159 Cas9 technology. We confirmed that *Dusp13* expression in skeletal muscle was depleted in these
160 *Dusp13* KO mice (Figure S2C). The *Dusp13* KO mice were born according to Mendelian laws and
161 grew normally, similar to the litter mate wild type (WT) control mice, with respect to body weight and
162 muscle cross-sectional area (CSA) of the soleus (SOL) and plantaris (PLA) muscles (Figure S3A–

163 S3C). We then investigated the regenerative ability in the *Dusp13* KO mice. We injected cardiotoxin
164 (CTX) into the tibialis anterior (TA) muscles of both WT and *Dusp13* KO mice and found no
165 significant histological differences in the CSA of the damaged myofibers with central nuclei at day 7
166 after the injury (Figure S3D and S3E). Furthermore, immunohistochemical analysis for PAX7 and
167 MYOGENIN showed that the number of PAX7 or MYOGENIN (+) nuclei was the same between WT
168 and *Dusp13* KO mice (Figure S3F–S3I). These findings indicate that there is no significant impairment
169 of muscle regeneration in the absence of *Dusp13*.
170 We hypothesized that other members of the *Dusp* family expressed in skeletal muscles could
171 compensate for the function of DUSP13 upon *Dusp13* deletion. Within overlapping genes between
172 the MyoD-KI Cluster 2 and MKO Cluster 2 in Figure 1A and 1B, we identified *Dusp27* as another
173 member of the *Dusp* family that is abundantly expressed in the quadriceps muscles and the heart
174 (Figure S2B). *Dusp27* expression was significantly higher in *Dusp13* KO muscles compared to WT
175 muscles, suggesting compensatory induction following the loss of *Dusp13* (Figure S4A). We also
176 observed a significant increase in *Dusp27* expression when *MyoD* expression increased (Figure S4B),
177 similar to *Dusp13* (Figure 1F). Interestingly, we found a potential Ebox site located 10 bp upstream of
178 the transcription initiation site of *Dusp27*, which is highly conserved among multiple mammalian
179 species (Figure S4C). The luciferase activity of luciferase-Dusp27-Ebox was significantly upregulated
180 in the presence of *MyoD* (Figure S4D), suggesting that both *Dusp13* and *Dusp27* are directly regulated
181 by MYOD activity. To test our hypothesis that DUSP27 compensates for the loss of *Dusp13*, we first
182 generated *Dusp27* KO mice using CRISPR-Cas9. We confirmed the deletion of the gene through
183 qPCR analysis (Figure S2D). Similar to the *Dusp13* KO mice, the *Dusp27* KO mice did not show any
184 differences in body weight (data not shown), muscle CSA before and after muscle CTX injury (Figure
185 S4E–S4J), or the number of myogenic populations labeled by either PAX7 or MYOGENIN after CTX
186 injury (Figure S4K–S4N). These results demonstrate that neither DUSP13 nor DUSP27 deficiency
187 influences muscle development and acute muscle regeneration.
188
189 ***Muscle regeneration is delayed in Dusp13:Dusp27 DKO mice.***
190 To investigate the role of DUSP13 and DUSP27 in skeletal muscles, we utilized DKO mice. The body
191 weights and muscle weights of DKO mice were found to be similar to age-matched WT mice (data
192 not shown). Furthermore, both the SOL and PLA muscles exhibited normal myofiber size (Figure
193 S5A–S5C), and the number of MuSCs was also normal (Figure S5D–S5G). However, histological
194 analysis on days 3, 7, and 28 after CTX injury clearly demonstrated the essential role of DUSP13 and
195 DUSP27 in muscle regeneration (Figure 2A–2D). Specifically, seven days post-injury, we observed a
196 notable increase in PAX7 (+) cells and a decrease in MYOGENIN (+) cells (Figure 2E–2H) in DKO
197 muscles compared to those in WT mice. At 28 days post-injury, when MuSCs are returning to their
198 niche after completing the muscle regeneration process, we observed a trend towards a reduction in

199 the number of PAX7 (+) cells (Figure S5H and S5I), accompanied by a notable increase in the number
200 of perduring MYOGENIN (+) cells undergoing regeneration (Figure S5J and S5K).
201 To confirm our *in vivo* findings indicating a severe delay in muscle regeneration in DKO mice, we
202 isolated MuSCs from DKO and WT mice using magnetic cell sorting (MACS) with α7-integrin
203 microbeads (Fujita et al., 2023; Sénéchal et al., 2022) and cultured them for three days (Figure 2I, 2J).
204 Immunofluorescent analysis using antibodies against PAX7 and MYOD showed a lower proportion
205 of differentiating PAX7 (-) and MYOD (+) cells in the DKO mice (Figure 2I, 2J)., indicating that
206 DUSP13/DUSP27 are necessary for the transition from activation to differentiation during myogenesis.
207 Since the lower differencing PAX7 (-), MYOD (+) cells in DKO mice, we observed a higher number
208 of proliferating Ki67 (+) MuSCs in DKO mice (Figure S6A–S6C). As expected, both myotube width
209 and fusion index exhibited a significant reduction in DKO mice relative to WT mice after six days of
210 MuSCs differentiation (Figure 2K–2M). These findings suggest that DUSP13 and DUSP27 dictate the
211 balance between the proliferation and differentiation of MuSCs during myogenesis.
212
213 ***Single-cell RNA sequencing revealed that Dusp13 and Dusp27 are highly expressed in the late***
214 ***differentiation stage of MuSCs.***
215 While MYOD activates *Dusp13* and *Dusp27* through their E-box, and *Dusp13*:*Dusp27* deficient mice
216 exhibit diminished muscle regeneration activity, the molecular mechanisms by which DUSP13 and
217 DUSP27 regulate myogenesis remain elusive. Additionally, the expression patterns of *Dusp13* and
218 *Dusp27* in different stages of myogenic progenitors within the highly heterogeneous MuSC
219 populations are not well-defined. In order to gain a more comprehensive understanding of the
220 molecular signatures of *Dusp13* and *Dusp27*-expressing myogenic cells, we conducted single-cell
221 RNA sequencing (scRNA-seq) on MyoD-high expressing cells isolated from cultured MuSCs
222 obtained from MyoD-KI mice (Figure 3A). This approach allowed us to enrich activated/differentiated
223 MyoD (+) cells (Fujita et al., 2023). MuSCs from MyoD-KI mice were cultured for five days in a
224 growth medium, and only live MyoD-high MuSCs with PI (-) negative populations were sorted by
225 fluorescence-activated cell sorter (FACS) for subsequent scRNA-seq library preparation (Figure 3A).
226 Utilizing the Seurat single-cell analysis package, we identified five distinct clusters of cells (C0–C4)
227 presented in the uniform manifold approximation and projection (UMAP) (Figure 3B). Each cluster
228 exhibited a unique transcriptomic fingerprint characterized by the top 10 differentially expressed genes
229 (Figure S7A).
230 To further understand the characteristics of these clusters, we conducted a Gene Ontology (GO)
231 analysis on differentially expressed genes (DEGs) among the clusters (Figure S7B–S7F). C0 and C4
232 showed upregulation of genes associated with chromosome segregation and DNA replication (Figure
233 S7B and S7F). C1 and C3 displayed strong enrichment for terms related to muscle differentiation,
234 maturation, and contraction (Figure S7C and S7E). C2 was characterized by genes associated with

ameboidal-type cell migration and extracellular organization (Figure S7D), akin to the previously reported MyoD-low MuSC signatures (Fujita et al., 2023). Next, we investigated cell cycle and myogenic markers, including *MKi67, E2f1, Ccnd1, Ccnd3, Pax7, Myf5, Myod1, Myogenin, Cdkn1c (p21), Myh3, Dusp13*, *and Dusup27* on UMAP (Figure 3C). *MyoD* is ubiquitously expressed across all clusters but with variations between the clusters (Figure 3C). *Mki67* and *E2f1*, which are proliferative markers, were highly expressed in C0 and C4 but not in C1, C2, and C3 (Figure 3C). Undifferentiated MuSC markers, *Pax7* and *Myf5*, were exclusively enriched in C0 and C2 (Figure 3C). Notably, *Dusp13* and *Dusp27* exhibited pronounced enrichment in C1 and C3, characterized by upregulation of genes associated with myogenic differentiation and maturation (Figure 3C). Considering the GO term and UMAP, C0 and C4 represent proliferative states, while C1 and C3 contain the differentiation and maturation state of MuSCs. On the other hand, C2 reflects the self-renewing MuSCs returning to the undifferentiated state. Furthermore, we used Monocle to analyze these MYOD-high expressing MuSC clusters and infer MuSC state trajectories (Figure 3D–3F). The cell state trajectory model revealed three branches for the MyoD-high-expressing MuSCs. These branches suggested that some clusters were transitioning towards further proliferation (C1, C4), myogenic differentiation/maturation (C1, C3), or self-renewal (C2) to return to an undifferentiated quiescent state (Figure 3D). We then focused the Monocle analysis on selected genes related to myogenic development/regeneration and cell cycle (*Pax7, Myf5, Myod1, Myogenin, Myf6, Myh3, Myh4, Hes6, Acta1, ccnd1, ccnd3, E2f1, Mki67, Cdkn1c (p21), Dusp13, and Dusp27*). Cluster 3 contained *Dusp13* and *Dusp27*, along with *Myogenin, Myh3, Hes6, Acta1,* and *Cdkn1c (p21)* (Figure 3E–3F). When visualizing the pseudotime progression axis of these selected genes, we observed that cells from C0 and C4, which expressed genes associated with the cell cycle (*Mki67* and *E2f1*) but had lower expression of *Pax7* and *Myf5*, were located at the initiation point of pseudotime (Figure 3E–3F). Cells from C2, which showed lower levels of *Mki67* and *E2f1* but higher levels of *Pax7*, *Myf5*, and *Ccnd1*, were mainly found in the middle point of pseudotime, suggesting that C2 represents a self-renewing MuSCs state (Brett et al., 2020; Fujita et al., 2023). In contrast, cells from C1 and C3, which highly expressed genes associated with myogenic differentiation and maturation, were located distally at the endpoint of pseudotime (Figure 3E and 3F), indicating myogenic differentiation and maturation states (Figure 3E and 3F). *Dusp13* and *Dusp27*, enriched in C1 and C3, progressed alongside myogenic differentiation markers and *Cdkn1c (p21)* (Figure 3E and 3F). Overall, the clustering and cell state trajectory analysis based on the scRNA-seq data of MyoD-high expressing MuSCs suggest that *Dusp13* and *Dusp27* are enriched only in the late stage of MyoD-positive MuSCs co-expressing *Myogenin*, *Myh3*, and *Cdkn1c*. They may regulate the switch from a proliferative state to a myogenic differentiation state.

Dusp13 drives precocious muscle differentiation through phosphatase activity in an independent manner.

Since our scRNA-seq analysis of MyoD-high expressing cells indicates that *Dusp13* and *Dusp27* are expressed in the subset of cells expressing late myogenic markers, such as myogenin. To investigate whether DUSP13 plays a role in initiating the differentiation process during myogenesis, we transduced FACS-isolated MuSCs from adult Pax7-YFP mice with an adenovirus vector expressing *Dusp13* or GFP under the CMV promoter (Figure 4A and Figure S8A and S8B). Two days post-infection, we observed a significant reduction in the number of MuSCs transduced with *Dusp13* compared to the GFP control (Figure 4B). Notably, immunofluorescent analysis using antibodies against PAX7 and MYOGENIN showed that *Dusp13* overexpression led to an induction of MYOGENIN expression in PAX7 (+) cells, which are typically not detected under normal culture conditions (Figure 4C and 4D). Furthermore, when we cultured MuSCs overexpressing *Dusp13* for seven days and assessed their myotube formation ability, we found that both the myotube width and fusion index were lower compared to the GFP control (Figure 4E–4G).

To investigate whether the phosphatase activity of DUSP13 is involved in myogenic induction, we transduced MuSCs from adult PAX7-YFP mice with pAd-Dusp13_Mut, which lacks enzymatic activity. Surprisingly, we discovered that DUSP13 without phosphatase activity still enhanced the population of PAX7 (+) and MYOGENIN (+) cells to the same extent as normal DUSP13 (Figure S8C and S8D). Taken together, these results suggest that DUSP13 acts as a driver for myogenin during myogenic progression, which is mediated by phosphatase activity-independent mechanisms.

DISCUSSION

Skeletal muscles have a remarkable capacity for regeneration, primarily relying on the activity of MuSCs. The regulation of MuSC dynamics involves the sequential expression of multiple transcription factors during myogenesis. MYOD plays a crucial role in determining the myogenic lineage specification during embryogenesis (Davis et al., 1987; Rudnicki et al., 1992, 1993). In adult mice regeneration, MYOD is induced in activated MuSCs, modulating the balance between self-renewal and differentiation (Megeney et al., 1996; Sabourin et al., 1999; White et al., 2000; Wood et al., 2013; Yablonka-Reuveni et al., 1999). However, the molecular mechanisms by which MYOD governs fate determination in MuSCs remain poorly understood. The diverse and highly heterogeneous nature of MuSCs, particularly during myogenesis, has posed a challenge in deciphering molecular signatures in MYOD-expressing MuSCs due to a lack of appropriate tools. This obstacle has hindered the elucidation of MYOD's role in fate determination. To address this, we previously engineered MyoD-KI mice, providing a platform to distinguish and isolate undifferentiated (MyoD-low) and committed MuSCs (MyoD-high).

305 In this study, we integrated our previously established whole transcriptome data encompassing
306 quiescent, undifferentiated (MyoD-low), and committed (MyoD-high) MuSCs from MyoD-KI
307 reporter mice (Fujita et al., 2023) with publicly available databases from *MyoD* KO mice (Wang et al.,
308 2022), Chip-atlas (Oki et al., 2018; Zou et al., 2022), and *MyoD* overexpression (Conerly et al., 2016).
309 Through this integration, we identified *Dusp13* as a novel molecular switch regulated by MyoD,
310 stimulating the initiation of myogenic differentiation. To understand the function of DUSP13, we
311 generated *Dusp13* KO mice using CRISPR-Cas9. Surprisingly, muscle development and regeneration
312 abilities in *Dusp13* KO mice mirrored those of their WT counterparts. This led us to investigate the
313 compensatory role of other members of the DUSP family. We found that *Dusp27* was also directly
314 regulated by MyoD. Although *Dusp27* KO mice generated in this study did not exhibit marked
315 differences in muscle development and regenerative ability following CTX injury, the combined
316 deficiency of *Dusp13* and *Dusp27* in mice resulted in substantial delays in muscle regeneration after
317 CTX injury. These findings suggest a compensatory interplay between DUSP13 and DUSP27 during
318 muscle regeneration. The quantities of PAX7 (+) quiescent MuSCs were identical between WT and
319 DKO mice before injury. However, at 28 days post-CTX injury, when muscle regeneration was almost
320 complete, DKO mice had lower levels of PAX7 (+) cells compared to WT mice. Conversely, DKO
321 mice had more MYOGENIN (+) cells remaining at day 28 post-injury compared to WT mice. At day
322 7 post-injury, DKO mice had higher numbers of PAX7 (+) cells and fewer MYOGENIN (+) cells.
323 These results suggest that the absence of *Dusp13* and *Dusp27* promotes the imbalance of the fate
324 determination processes in MuSCs following muscle injury. *In vitro* analyses employing isolated
325 MuSCs from DKO mice supported these findings, showing that the absence of *Dusp13* and *Dusp27*
326 promotes proliferation rather than differentiation. Consequently, the delay/failure in transitioning from
327 the activation/proliferation phases to differentiation, attributed to the deficiency of *Dusp13* and
328 *Dusp27*, disrupts the muscle repair process in adult mice.
329 To further investigate the regulatory dynamics of *Dusp13* and *Dusp27* in fate determination, we
330 conducted scRNA-seq on MyoD-high expressing MuSCs isolated from MyoD-KI mice. Intriguingly,
331 both *Dusp13* and *Dusp27* expression were enriched in specific clusters (C1 and C3) within the MyoD-
332 high expressing MuSC populations. These clusters were characterized by increased expression of late
333 myogenic markers, such as *Myogenin, Myh3,* and *Cdkn1a*, and decreased expression of *Pax7*, *MKi67*,
334 and *Myf5*. Pseudotime cell state trajectory analysis was used to distinguish the fate determination of
335 MuSCs during myogenesis. Cluster C0 represented a proliferative state with high expression of
336 undifferentiated markers (*Pax7* and *Myf5*) and cell cycle markers (*MKi67* and *E2f1*), which projected
337 to further proliferate (C4), differentiate/mature (C1 and C3), or self-renew to return to an
338 undifferentiated quiescent state (C2). We believe that the scRNA-seq data from our MyoD-KI mice
339 will provide a valuable resource for uncovering new molecular mechanisms involved in myogenic fate

340 transition (proliferation, differentiation, or self-renewal/quiescence) of activated MuSCs during
341 myogenesis.
342 Given the limited expression of *Dusp13* and *Dusp27* in C1 and C3, we hypothesized that these two
343 genes play a crucial role in the transition from proliferation to differentiation. In our study, we
344 overexpressed *Dusp13* in MuSCs using an adenovirus vector. While the expression of PAX7 and
345 MYOGENIN expression is typically mutually exclusive during myogenesis (Olguin et al., 2007), a
346 small subset of cells does exhibit positivity for both PAX7 and MYOGENIN, representing an
347 intermediate population initiating differentiation (Halevy et al., 2004). In our model, a limited number
348 of PAX7 (+) and MYOGENIN (+) cells were also identified. Notably, *Dusp13* overexpression
349 significantly augmented the population of PAX7 (+) and MYOGENIN (+) cells. Collectively, our
350 findings align with the scRNA-seq analysis results, supporting the notion that the MYOD-DUSP13
351 and DUSP27-MYOGENIN regulatory network governs the initiation of differentiation for muscle
352 regeneration in adult mice.
353 There are limited studies on the regulatory roles of the DUSP family in myogenesis. Therefore,
354 the molecular targets modulated by DUSP13 and DUSP27 in MuSCs are currently unknown. The
355 DUSPs family possesses the dual ability to dephosphorylate phosphor-serine/threonine and phospho-
356 tryosoine residues. Currently, 25 different DUSPs are identified and categorized into six subfamilies
357 (Alonso and Pulido, 2016). DUSP13, an atypical DUSP, has versatile dephosphorylation substrates,
358 including mitogen-activated protein kinases (MAPKs). Forced expression of pAd-Dusp13_Mut vector,
359 without phosphatase activity, into MuSCs led to the emergence of PAX7 (+) and MYOGENIN (+)
360 cells *in vitro*, indicating phosphatase-independent mechanisms mediated by DUSP13 for myogenic
361 differentiation. Interestingly, DUSP27 is recognized as a pseudo-phosphatase, characterized by
362 catalytically inactive phosphatase activity. Various pseudo-phosphatases are reported to possess
363 pivotal functions in different organisms and pathological conditions (Reiterer et al., 2020). Inhibition
364 of ERK1/2 promotes myogenic differentiation and fusion in both mice and avian models (Eigler et al.,
365 2021). The DUSP family, lacking a kinetic-interacting motif, inhibits ERK1/2 signaling (Hu and
366 Mivechi, 2006; Huang et al., 2000; Marti et al., 2001), suggesting that the phosphatase-independent
367 activities of DUSP13 and DUSP27 potentially regulate ERK signaling in MuSCs. Future
368 investigations are expected to unravel the detailed molecular mechanisms by which DUSP13 and
369 DUSP27 orchestrate fate switching in activated MuSCs during myogenesis.
370 In summary, using our previously established MyoD-KI mice model, we identified *Dusp13* and
371 *Dusp27* as novel MYOD target genes that play a pivotal role in the fate switching of MuSCs.
372 Furthermore, we demonstrated that *Dusp13* and *Dusp27* expressions are highly enriched in
373 differentiation clusters revealed by scRNA-seq of MyoD-high expressing MuSCs. Beyond both being
374 new determinants for the initiation of myogenic differentiation, further analysis of scRNA-seq data
375 within each cluster will yield valuable insights into identifying more potent fate determinants in

376 MuSCs during myogenesis.
377
378 ***Limitation of the study***
379 Although our study shows that DKO mice have reduced muscle regeneration ability, there are certain
380 limitations that need to be taken into account in the interpretation of our results, given that *Dusp13*
381 and *Dusp27* deletion is systemically induced. To further investigate muscle regeneration, we isolated
382 MuSCs from DKO mice and found that they exhibited impaired myotube formation compared to WT
383 mice. However, optimal regeneration requires coordination among multiple cell types, including
384 inflammatory cells (Arnold et al., 2007; Fujita et al., 2014) and fibro-adipogenic progenitors (Joe et
385 al., 2010; Uezumi et al., 2010). The expression of *Dusp13* and *Dusp27* is comparatively lower in other
386 tissues than in skeletal muscles (Figure S2A–S2B). Nevertheless, further investigations are necessary
387 to reveal the inflammatory status in DKO mice both before and after injury. Under normal conditions,
388 the size, weight, and histology of skeletal muscles in DKO mice are indistinguishable from those in
389 WT mice. The reason why the loss of *Dusp13* and *Dusp27* does not affect muscle development during
390 embryonic development is unclear. It is possible that other members of the DUSP family might
391 compensate for their roles in embryonic and postnatal muscle formation, or the downstream targets of
392 DUSP13 and DUSP27 may diverge between muscle regeneration and embryonic myogenesis. Our
393 demonstration of *Dusp13* overexpression promoting MYOGENIN in PAX7(+) MuSCs indicates
394 precocious differentiation. Moreover, our scRNA-seq data of MyoD-high MuSCs clearly show that
395 the late myogenic stage MyoD-positive MuSCs express *Dusp13* and *Dusp27*. Expanding on the
396 molecular functions of the genes within these clusters will contribute to deciphering the molecular
397 targets of DUSP13 and DUSP27.

Acknowledgments

We would like to thank Satoshi Yamazaki and Yuji Yamazaki from the Division of Stem Cell Therapy, University of Tsukuba, for their valuable technical assistance in cell sorting using flow cytometry. This work was supported by a grant from the MEXT Leading Initiative for Excellent Young Researchers (R.F.), and the Grant-in-Aid for Early-Career Scientists (21K17679; R.F.). This work was also supported, in part, by grants to R.F. from the Takeda Science Foundation and Mochida Memorial Foundation for Medical and Pharmaceutical Research. T.H. and S.S were funded by JSPS Research Fellowships for Young Scientists (22J10954 (T.H.) and 23KJ0287 (S.S.)). Furthermore, this work received support from the Grant-in-Aid for the Japan Aerospace Exploration Agency (14YPTK-407 005512; S.T.) and the Grant-in-Aid for Scientific Research on Innovative Area from MEXT (18H04965; S.T.).

Author contributions

T.H., S.M., S.T., and R.F. conceived the study and designed the experiments. T.H., S.S., R.T., R.O., S.F., M.K., A.N., Y.O., M.M., S.M., D.S., E.W., T.K., and R.F. performed the experiments and bioinformatic analysis. T.H., G.W., T.S., and R.F. performed single-cell RNA-seq analysis. T.H., S.T., and R.F. wrote the manuscript. All authors contributed to the analysis and interpretation of results and reviewed the manuscript.

Competing interests

The authors declare no competing financial interests.

Additional information

Supplementary information

Supplementary Information is available for this paper.

Corresponding authors

Correspondence and requests for materials should be addressed to Ryo Fujita.

STAR METHODS

RESOURCE AVAILABILITY

Lead contact

Further information and request for reagents may be directed to and will be fulfilled by the lead contact, Ryo Fujita (fujiryo@md.tsukuba.ac.jp).

Materials availability

All unique reagents generated in this study are available from the lead contact in accordance with the relevant material transfer agreements.

Data and code availability

- Single-cell RNA-seq data have been deposited in the NCBI Gene Expression Omnibus (GEO). The accession number is listed in the key resources table.
- This paper does not report original code.
- Any additional information required to reanalyze the data reported in this paper is available from the lead contact upon request.

EXPERIMENTAL MODELS AND SUBJECT DETAILS

Mice

Mice were kept in a specific pathogen-free environment at the Laboratory Animal Resource Center at the University of Tsukuba, Ibaraki, Japan. All experiments were performed in compliance with the relevant Japanese and institutional laws and guidelines and were approved by the University of Tsukuba Animal Ethics Committee (authorization number: 23-046). The study used male and female WT, *Dusp13* KO, *Dusp27* KO, *Dusp13*/*Dusp27* DKO mice, unless otherwise stated. Quiescent MuSCs were directly isolated from the leg muscles of 15–16-week-old male Pax7-YFP (*Pax7*$^{YFP/YFP}$) (Kitajima and Ono, 2018) (Fujita et al., 2023). The TA muscle was acutely injured by injecting 50 µL of 10 µM cardiotoxin (Funakoshi Co., Ltd., Tokyo, Japan) under anesthesia using isoflurane inhalation.

METHOD DETAILS

Generation of *Dusp13* and *Dusp27* KO mice

The *Dusp13* and *Dusp27* KO mice were generated using the CRISPR/Cas9 system. Two target sgRNAs were designed as follows; 5′-GTAGGGTTCACACAGAACGG-3′ and 5′-ATGTCACAGTAAGCGTACGG-3′ for targeting all exons of the *Dusp13* gene on mouse chromosome 14, and 5′-GCATCCTTCCACATCAACCC-3′ and 5′-GGTAAGGGTGCTCTCGACAA-3′ for targeting regions located in introns 2 and 3, respectively, of

462 the *Dusp27* gene on mouse chromosome 1. Each target sgRNA was cloned into the guide RNA-Cas
463 co-expression plasmid px330-U6-Chimeric_BB-CBh-hSpCas9 vector (Addgene, Watertown, MA,
464 USA). A mixture of the four cloned plasmids was microinjected into the pronuclei of C57BL/6 J
465 fertilized eggs, and living embryos were transferred to pseudo-pregnant ICR female mice. Genomic
466 DNA screening was performed using PCR with the primers and protocols listed in Table S1.
467

468 **Muscle stem cell isolation and culture**

469 MuSCs were isolated from the hindlimb muscles of 11–13-week-old mice following MACS using a
470 Satellite Cell Isolation Kit (Miltenyi Biotec, Bergisch Gladbach, Germany) and anti-integrin α7
471 microbeads (Miltenyi Biotec), as previously described (Fujita et al., 2023). The adult hindlimb
472 muscles were minced in ice-cold Ham's F12 medium. The minced muscles were then incubated in
473 0.1% collagenase D (Roche, Basel, Switzerland) and 0.1% trypsin in Ham's F12 (Gibco, Waltham,
474 MA, USA) with 1% penicillin-streptomycin for 45 min at 37 °C on a shaker for three rounds of
475 digestion. After each round, the supernatant was collected in a 50 mL tube containing 8 mL of fetal
476 bovine serum (FBS) (Gibco) on ice, and fresh 0.1% trypsin/0.1% collagenase digestion buffer was
477 added to the tube for the next round of digestion. The collected supernatant was filtered through a
478 sequence of 100 and 40 μm nylon mesh strainers and then centrifuged at 400 × *g* for 10 min at 4 °C.
479 The pellets were resuspended in PBS containing 2% FBS and processed for MACS or flow cytometry.
480 The MuSCs were cultured in a growth medium containing 39% DMEM (Gibco), 39% Ham's F12,
481 20% FBS (Gibco), and 1% UltroserG (Pall Life Sciences, Port Washington, NY, USA). Differentiation
482 media consisted of 2% horse serum in Dulbecco's modified Eagle's medium (DMEM). Gelatin (0.2%)-
483 coated dishes were used for MuSC culture unless otherwise indicated.
484

485 **Immunofluorescence and histological analysis**

486 Cultured cells were washed twice with PBS after removing the media and fixed with 4%
487 paraformaldehyde (PFA) for 15 minutes. The fixed cells were blocked with 2% BSA/PBS for 1 hour
488 at room temperature and then washed three times with PBS. Isolated single EDL myofibers (Sénéchal
489 et al., 2022) were fixed using 2% PFA for 15 min, permeabilized with 0.1% Triton in PBS, and blocked
490 with 5% goat serum in 0.1% Triton/PBS for 30 min on a shaker. The cultured cells and single EDL
491 myofibers were incubated with primary antibodies at 4 °C overnight. The myotube diameter and
492 nucleus number were measured using the ImageJ software (NIH, Bethesda, MI, USA). The myotube
493 diameter was defined as the average diameter at the three ends (both ends and the center) for each
494 MYHC-positive and multinucleated myotube. TA muscles were neatly stacked on top of each other.
495 The Achilles tendon side was vertically mounted on tragacanth gum on a cork disc and quickly frozen
496 in isopentane cooled in liquid nitrogen. Thin frozen muscle sections (8 μm) were subjected to
497 immunohistochemical analyses. The sections were fixed with 4% PFA for 10 min at room temperature.

498 For PAX7 staining, sections underwent antigen retrieval with DAKO buffer (Agilent, Santa Clara, CA,
499 USA) for 10 min at 110 °C, followed by blocking with M.O.M. blocking reagent (Vector Laboratories,
500 Newark, CA, USA). The sections were then incubated with primary antibodies overnight at 4 °C.
501 Tissue sections were mounted with VECTASHIELD Vibrance Antifade Mounting Medium with
502 DAPI (Vector Laboratories). Primary antibodies were against PAX7 (Developmental Studies
503 Hybridoma Bank (DSHB)), MyoD (sc-377460; SantaCruz), LAMININ (sc-59854; SantaCruz),
504 MYOGENIN (124800; Abcam, Cambridge, UK), MYHC (DSHB; MF20), and KI67 (MA5-14520;
505 Invitrogen, Waltham, MA, USA). For immunofluorescence, secondary antibodies conjugated with
506 Alexa Fluor-488, Alexa Fluor-546, Alexa Fluor-555, Alexa Fluor-633, and Alexa Fluor-647 were used.
507 The secondary antibodies included anti-mouse IgG1, anti-mouse IgG2b, anti-rat IgG, and anti-rabbit
508 antibodies (Thermo Fisher Scientific, Waltham, MA, USA). For HE staining, the SOL, PLA, and TA
509 muscle sections were stained with Mayer's hematoxylin (Wako, Richmond, VA, USA) for 10 min.
510 After washing in warm running tap water (50 ± 5 °C) for 3 minutes, eosin (Wako) was applied for 1
511 min. The sections were then dehydrated using two changes (5 s each) of 95% ethanol and two changes
512 (5 s each) of 100% ethanol (Wako), followed by three changes of xylene (Wako) for 5 min each.
513 Finally, the sections were mounted with DPX mounting medium (Sigma-Aldrich, St. Louis, MA,
514 USA) and observed with a BIOREVO BZ-X800 microscope (Keyence, Osaka, Japan). The CSA of
515 myofibers was assessed using the same microscope system and a hybrid cell count application
516 (Keyence).
517
518 **Flow cytometry analysis and cell sorting**
519 MACS-isolated MuSCs were cultured for 5 days. They were detached using 0.25% trypsin/EDTA,
520 then centrifuged and resuspended in 2% FBS/PBS. Propidium iodide (PI) was added to the cells at a
521 1:500 (vol/vol) ratio and incubated on ice for 10 min. The cells were either analyzed using a flow
522 cytometer (CytoFLEX S; Beckman Coulter, Brea, CA, USA) or sorted using a MoFlo XDP flow
523 cytometer (Beckman Coulter). Debris and dead cells were excluded using forward scatter, side scatter,
524 and PI gating. Gates were defined based on WT control fluorescence. The data were analyzed using
525 FlowJo™ software ver. 10.7.1 (BD Biosciences, Franklin Lakes, NJ, USA).
526
527 **DNA construct**
528 The *MyoD*, *Dusp13*, and *Dusp27* genes were amplified using PrimeStar GXL DNA Polymerase
529 (Takara Bio, Shiga, Japan) with soleus cDNA as the template. After confirming the size of the PCR
530 products using 1% agarose gel electrophoresis, the target PCR product was purified from the gel. The
531 purified DNA fragment of *Dusp13* was digested with EcoRI. The digested fragments were then ligated
532 to pENTR3c-IRES-EGFP, which was also digested with the same restriction enzymes, using Ligation
533 High (TOYOBO, Osaka, Japan). DUSP13 deficient in phosphatase activity (=Dusp13_Mut) was

534 generated using the PrimeSTAR® Mutagenesis Basal Kit (Takara Bio). The Dusp family contains the
535 amino acid cysteine, which is essential for enzyme activity (Alonso et al., 2004). The present mutant
536 was generated using Dusp13_D97A and Dusp13_C128S primers (Table S1) to replace aspartic acid
537 at position 97 and cysteine at position 128 with alanine and serine, respectively. The reaction was then
538 transformed into One shot TOP10 Competent cells (Thermo Fisher Scientific) and seeded on
539 kanamycin-LB agar plates. A single colony was grown in kanamycin-LB medium, and after
540 confirming each insert by colony PCR and DNA sequencing, plasmid purification was performed
541 using the FastGene Plasmid Mini Kit. Clones without any mutations in the product were selected. The
542 LR reaction of the Gateway system was performed to recombine pENTR3c-Dusp13-IRES-EGFP into
543 pAd/CMV/V5-DEST (Thermo Fisher Scientific). In total, 100 ng of the purified plasmid and 300 ng
544 of pAd/CMV/V5-DEST were mixed at room temperature and reacted according to the manual for
545 Gateway LR Clonase II Enzyme Mix (Thermo Fisher Scientific). The 5 μL reaction was subsequently
546 transformed into 50 μL of competent cells and seeded on ampicillin-LB agar plates. Single colonies
547 were cultivated in LB medium, and confirmation of the insert was achieved through colony PCR. The
548 confirmed plasmid was prepared in large quantities using the PureLink HiPure Plasmid Midiprep Kit
549 (Thermo Fisher Scientific). The plasmid concentration was measured using a NanoDrop 2000
550 Spectrophotometer (Thermo Fisher Scientific), and 20 μg of the plasmid was digested with the
551 restriction enzyme PacI. Verification of complete digestion by PacI was performed through 1%
552 agarose gel electrophoresis, and the linearized plasmid was purified via phenol:chloroform extraction
553 and ethanol precipitation. To generate the luciferase vector, the purified DNA fragment of the *MyoD*
554 gene was cloned into a pAAV-CMV vector using the In-Fusion Cloning HD Kit (Takara Bio). The
555 DNA fragment corresponding to the 300 bp 5′ upstream region (−250 to +50) of *Dusp13* or the 1,200
556 bp upstream region (−1,000 to +200) of *Dusp27* from EDL muscle DNA of C57BL/6 mice was
557 inserted into a pGL4.10 promoter-less luciferase vector (Promega, Madison, WI, USA) digested with
558 XhoI. The resulting constructs were named pGL4-Dusp13 or pGL4-Dusp27. The primer sequences
559 for the construction of vectors are provided in Table S1.
560

561 **Adenovirus production and infection**

562 293A cells were seeded on BD BioCoat Collagen I 60 mm Culture Dishes (IWAKI) using the medium
563 (DMEM and 10% FBS). Purified 5 μg of pAd/CMV/V5-DEST plasmid was transfected using Fugene
564 HD (Promega) when the 293A cells were 80% confluent. When the cells began to float, the bottom
565 surface of the dish was scraped off using a scraper and collected in a 15 mL High-Clarity
566 Polypropylene Conical Tube 17 × 120 mm style (FALCON) (primary virus). The primary virus
567 underwent repeated freeze-thaw cycles in a water bath at 37 °C and in liquid nitrogen. This freeze-
568 thaw process was repeated three times. Finally, it was frozen again and stored at −80 °C. Next, 2 mL
569 of the primary virus was thawed at 37 °C and centrifuged for 15 min at 3,000 rpm (KUBOTA 2800).

570 The supernatant was added to 293A cells (80% confluent) cultured in a 100 mm Collagen-Coated Dish
571 Collagen I (IWAKI) and infected for 1 hour at 37 °C in a CO_2 incubator. Then, 8 mL of medium was
572 added. When the cells floated, they were scraped off using a scraper and collected in 15-mL tubes.
573 The freeze-thaw process was repeated three times. Finally, it was frozen again and stored at −80 °C.
574 This virus was created as the 2nd virus. This procedure was repeated five times, and the 5th virus was
575 stored at −80 °C. Next, to purify the virus, the fifth virus was freeze-thawed three times and
576 ultracentrifuged at 23 k rpm at 4 °C for 1.5 hours in the Super-centrifuge Optima XE-90
577 Ultracentrifuge (Beckman Coulter) using Ultra-Clear Centrifuge Tubes (Beckman Coulter). After
578 ultracentrifugation, recombinant adenovirus was extracted from the second viral layer from the bottom.
579 The dialysis buffer was prepared in three heat-resistant plastic bottles by adding 1976 mL of MilliQ,
580 20 mL of 1 M Tris HCl (pH 8.0), and 4 mL of 1 M $MgCl_2$, and the bottles were then autoclaved. For
581 dialysis, the recombinant adenovirus extract was injected into Slide-A-Lyzer Dialysis Cassettes
582 (Thermo Fisher Scientific) and dialyzed in a dialysis buffer at 4 °C with stirring. The dialysis buffer
583 was changed three times every 12 hours. The purified recombinant adenovirus was stored at −80 °C.
584 Infectious titers were measured using the Adeno-X Rapid Titer Kit (Takara Bio). MuSCs were
585 cultured in a growth medium (GM) composed of DMEM (Gibco, high glucose, 11960-044), 10% FBS,
586 1% Pen Strep (Gibco), and 2 mM L-glucose (Gibco) at 37 °C under 5% CO_2. To differentiate into
587 myotube cells, cells were seeded at 1×10^4 cells/well (12-well plate). Differentiation was induced by
588 replacing the growth medium with a differentiation medium (DM) consisting of DMEM, 2% horse
589 serum (Gibco), 1% Pen Strep (Gibco), and 2 mM L-glucose (Gibco). After 48 hours from the start of
590 differentiation, the medium was replaced with a fresh DM and incubated with adenovirus at a
591 multiplicity of infection (MOI) of 250 in a differentiation medium. Two days after the virus
592 transduction, the cells were fixed with 4% PFA/PBS and permeabilized with 0.1% Triton X-100/PBS.
593 The fixed cells were blocked with 2% BSA/PBS for 1 h at room temperature and washed three times
594 with PBS. The myotube cells were then reacted with monoclonal anti-PAX7 antibody (DSHB) (1:100)
595 and anti-MYOGENIN (ab124800; Abcam) (1:100) in 2% BSA/PBS at 4 °C overnight. After washing
596 with PBS, they were incubated with appropriate Alexa Fluor-conjugated secondary antibodies
597 (Thermo Fisher Scientific) for 1 hour at room temperature and mounted with 20 mM Tris and 90%
598 glycerol. The detection was photographed with a fluorescence microscope BIOREVO (BZ-X800;
599 Keyence).
600
601 **Luciferase assay**
602 To determine if MyoD could activate the *Dusp13* or *Dusp27* promoter, we co-transfected 100 ng of
603 pGL4-Dusp13 or pGL4-Dusp27 with 50 ng of pRL-TK vectors (Promega) and varying amounts (0,
604 10, 20, 100, 200 ng) of pAAV MyoD expression vectors into AAVpro 293T cells (Takara Bio) using
605 the FuGENE HD transfection reagent (Promega). Twenty-four hours after transfection, the cells were

606 harvested and assayed using the Dual-Luciferase Reporter Assay System (Promega). Luciferase
607 activity was measured using the GloMax® 20/20 Luminometer (Promega) and normalized based on
608 Renilla luciferase activity from the pRL-TK vector.
609
610 **Motif enrichment analysis**
611 The presence of Ebox sites in the promoter regions of genes was predicted using the Find Individual
612 Motif Occurrences (FIMO) algorithm from the MEME Suite (Grant et al., 2011), utilizing the position
613 weight matrix available from JASPAR (https://jaspar.genereg.net/). This analysis was conducted from
614 1 kbp upstream to 500 bp downstream of the transcriptional start site of *Dusp13*/*Dusp27*.
615
616 **RNA isolation and RT-qPCR**
617 Total RNA was extracted from various tissues and MuSCs using ISOGEN (NIPPON GENE, Chiyoda,
618 Tokyo, Japan). We synthesized first-strand cDNA using the QuantiTect Reverse Transcription Kit
619 (Qiagen, Hilden, Germany). Polymerase chain reaction (PCR) was then performed using a
620 THUNDERBIRD SYBR qPCR system (TOYOBO) and a TP850 Thermal Cycler Dice Real Time
621 System (Takara Bio, Shiga, Japan). The primer sequences are listed in Table S1. The relative amount
622 of each transcript was normalized to the number of beta-actin transcripts.
623
624 **Single-cell RNA-seq analysis**
625 MACS-isolated MuSCs from MyoD-KI mice (Fujita et al., 2023) were cultured for five days and then
626 detached using 0.25% trypsin/EDTA. The cells were centrifuged and resuspended in 2% FBS/PBS.
627 The cells were incubated with PI at a 1:500 (v/v) ratio. Debris and dead cells were excluded using
628 forward scatter, side scatter, and PI gating. Live MyoD-tdTomato-high MuSCs were sorted using a
629 MoFlo XDP flow cytometer (Beckman Coulter) based on our previous study's gate of MyoD-
630 tdTomato-high population. Single RNA-seq libraries from MyoD-tdTomato-high MuSCs were
631 generated using a chromium controller (10× Genomics, Pleasanton, CA, USA) following the
632 manufacturer's instructions. Approximately 10,000 cells were processed using the Chromium Next
633 GEN Single Cell 3'Reagent Kits v3.1 (10× Genomics). The sequencing was performed on a NovaSeq
634 6000 (Illumina, San Diego, CA, USA) operated by the Rhelixa Corporation (Tokyo, Japan). The fastq
635 files were processed using default parameters for adaptor sequence filtering, and low-quality reads
636 were removed to obtain clean data. Feature-barcode matrices were then generated by aligning the reads
637 to the mouse genome (mm10 Ensemble: version 92) with CellRanger v3.1.0. The scRNA-seq data
638 was processed using the standard Seurat pipeline. For quality control, the range of gene reads per cell
639 was set between 300 and 6000. Additionally, the filtering threshold for mitochondrial gene proportion
640 was established at 15%. The "FindVariableFeature" function was used to determine the highly variable
641 genes. Cell clustering was determined using the "FindNeighbors" and "FindCluster" functions in the

Seurat package. To investigate the proliferation of genes involved in the development of muscle stem cells, the "Monocle2" package was applied for conducting pseudotime analysis. The biological function analysis was performed using GO analysis.

Quantification and statistical analysis

All data are represented as the mean of biological replicates, with individual sample data shown as dots. Values are reported as mean ± standard error of the mean (SEM). Statistical analyses were performed using unpaired Student's t-tests or non-repeated measures analysis of variance (ANOVA), followed by Tukey's test, using GraphPad Prism (GraphPad Software, Inc., San Diego, CA, USA). P values for statistical significance are indicated as * $P < 0.05$, ** $P < 0.01$, *** $P < 0.001$, not detected (n.d.), or not significant (n.s.).

653 **References**

654 Alonso, A., and Pulido, R. (2016). The extended human PTPome: a growing tyrosine
655 phosphatase family. FEBS J *283*, 1404–1429. https://doi.org/10.1111/febs.13600.
656 Alonso, A., Sasin, J., Bottini, N., Friedberg, I., Friedberg, I., Osterman, A., Godzik, A.,
657 Hunter, T., Dixon, J., and Mustelin, T. (2004). Protein tyrosine phosphatases in the
658 human genome. Cell *117*, 699–711. https://doi.org/10.1016/j.cell.2004.05.018.
659 Aoki, N., Aoyama, K., Nagata, M., and Matsuda, T. (2001). A growing family of dual
660 specificity phosphatases with low molecular masses. J Biochem *130*, 133–140.
661 https://doi.org/10.1093/oxfordjournals.jbchem.a002952.
662 Arnold, L., Henry, A., Poron, F., Baba-Amer, Y., van Rooijen, N., Plonquet, A.,
663 Gherardi, R.K., and Chazaud, B. (2007). Inflammatory monocytes recruited after
664 skeletal muscle injury switch into antiinflammatory macrophages to support
665 myogenesis. Journal of Experimental Medicine *204*, 1057–1069.
666 https://doi.org/10.1084/jem.20070075.
667 Bermudez, O., Pagès, G., and Gimond, C. (2010). The dual-specificity MAP kinase
668 phosphatases: critical roles in development and cancer. Am J Physiol Cell Physiol *299*,
669 C189-202. https://doi.org/10.1152/ajpcell.00347.2009.
670 Boyer, J.G., Prasad, V., Song, T., Lee, D., Fu, X., Grimes, K.M., Sargent, M.A.,
671 Sadayappan, S., and Molkentin, J.D. (2019). ERK1/2 signaling induces skeletal muscle
672 slow fiber-type switching and reduces muscular dystrophy disease severity. JCI Insight
673 *4*, e127356. https://doi.org/10.1172/jci.insight.127356.
674 Brett, J.O., Arjona, M., Ikeda, M., Quarta, M., De Morrée, A., Egner, I.M., Perandini,
675 L.A., Ishak, H.D., Goshayeshi, A., Benjamin, D.I., et al. (2020). Exercise rejuvenates
676 quiescent skeletal muscle stem cells in old mice through restoration of Cyclin D1. Nat
677 Metab *2*, 307–317. https://doi.org/10.1038/s42255-020-0190-0.
678 Chen, H.-H., Luche, R., Wei, B., and Tonks, N.K. (2004). Characterization of two
679 distinct dual specificity phosphatases encoded in alternative open reading frames of a
680 single gene located on human chromosome 10q22.2. J Biol Chem *279*, 41404–41413.
681 https://doi.org/10.1074/jbc.M405286200.
682 Collins, C.A., Olsen, I., Zammit, P.S., Heslop, L., Petrie, A., Partridge, T.A., and
683 Morgan, J.E. (2005). Stem cell function, self-renewal, and behavioral heterogeneity of
684 cells from the adult muscle satellite cell niche. Cell *122*, 289–301.
685 https://doi.org/10.1016/j.cell.2005.05.010.
686 Conerly, M.L., Yao, Z., Zhong, J.W., Groudine, M., and Tapscott, S.J. (2016). Distinct
687 Activities of Myf5 and MyoD Indicate Separate Roles in Skeletal Muscle Lineage

688 Specification and Differentiation. Dev Cell *36*, 375–385.
689 https://doi.org/10.1016/j.devcel.2016.01.021.
690 Crist, C.G., Montarras, D., and Buckingham, M. (2012). Muscle satellite cells are
691 primed for myogenesis but maintain quiescence with sequestration of Myf5 mRNA
692 targeted by microRNA-31 in mRNP granules. Cell Stem Cell *11*, 118–126.
693 https://doi.org/10.1016/j.stem.2012.03.011.
694 Davis, R.L., Weintraub, H., and Lassar, A.B. (1987). Expression of a single transfected
695 cDNA converts fibroblasts to myoblasts. Cell *51*, 987–1000.
696 https://doi.org/10.1016/0092-8674(87)90585-X.
697 Denu, J.M., and Dixon, J.E. (1995). A catalytic mechanism for the dual-specific
698 phosphatases. Proc Natl Acad Sci U S A *92*, 5910–5914.
699 https://doi.org/10.1073/pnas.92.13.5910.
700 Denu, J.M., and Dixon, J.E. (1998). Protein tyrosine phosphatases: mechanisms of
701 catalysis and regulation. Curr Opin Chem Biol *2*, 633–641.
702 https://doi.org/10.1016/s1367-5931(98)80095-1.
703 Eigler, T., Zarfati, G., Amzallag, E., Sinha, S., Segev, N., Zabary, Y., Zaritsky, A.,
704 Shakked, A., Umansky, K.-B., Schejter, E.D., et al. (2021). ERK1/2 inhibition promotes
705 robust myotube growth via CaMKII activation resulting in myoblast-to-myotube fusion.
706 Developmental Cell *56*, 3349-3363.e6. https://doi.org/10.1016/j.devcel.2021.11.022.
707 Fero, K., Bergeron, S.A., Horstick, E.J., Codore, H., Li, G.H., Ono, F., Dowling, J.J.,
708 and Burgess, H.A. (2014). Impaired embryonic motility in dusp27 mutants reveals a
709 developmental defect in myofibril structure. Dis Model Mech *7*, 289–298.
710 https://doi.org/10.1242/dmm.013235.
711 Fujita, R., Kawano, F., Ohira, T., Nakai, N., Shibaguchi, T., Nishimoto, N., and Ohira,
712 Y. (2014). Anti-interleukin-6 receptor antibody (MR16-1) promotes muscle
713 regeneration via modulation of gene expressions in infiltrated macrophages. Biochimica
714 et Biophysica Acta (BBA) - General Subjects *1840*, 3170–3180.
715 https://doi.org/10.1016/j.bbagen.2014.01.014.
716 Fujita, R., Zismanov, V., Jacob, J.-M., Jamet, S., Asiev, K., and Crist, C. (2017). Fragile
717 X mental retardation protein regulates skeletal muscle stem cell activity by regulating
718 the stability of Myf5 mRNA. Skeletal Muscle *7*, 18. https://doi.org/10.1186/s13395-
719 017-0136-8.
720 Fujita, R., Mizuno, S., Sadahiro, T., Hayashi, T., Sugasawa, T., Sugiyama, F., Ono, Y.,
721 Takahashi, S., and Ieda, M. (2023). Generation of a MyoD knock-in reporter mouse line
722 to study muscle stem cell dynamics and heterogeneity. iScience *26*, 106592.
723 https://doi.org/10.1016/j.isci.2023.106592.

724 Grant, C.E., Bailey, T.L., and Noble, W.S. (2011). FIMO: scanning for occurrences of a
725 given motif. Bioinformatics *27*, 1017–1018.
726 https://doi.org/10.1093/bioinformatics/btr064.
727 Halevy, O., Piestun, Y., Allouh, M.Z., Rosser, B.W.C., Rinkevich, Y., Reshef, R.,
728 Rozenboim, I., Wleklinski-Lee, M., and Yablonka-Reuveni, Z. (2004). Pattern of Pax7
729 expression during myogenesis in the posthatch chicken establishes a model for satellite
730 cell differentiation and renewal. Developmental Dynamics *231*, 489–502.
731 https://doi.org/10.1002/dvdy.20151.
732 Hausburg, M.A., Doles, J.D., Clement, S.L., Cadwallader, A.B., Hall, M.N.,
733 Blackshear, P.J., Lykke-Andersen, J., and Olwin, B.B. (2015). Post-transcriptional
734 regulation of satellite cell quiescence by TTP-mediated mRNA decay. eLife *4*, e03390.
735 https://doi.org/10.7554/eLife.03390.
736 Hu, Y., and Mivechi, N.F. (2006). Association and regulation of heat shock
737 transcription factor 4b with both extracellular signal-regulated kinase mitogen-activated
738 protein kinase and dual-specificity tyrosine phosphatase DUSP26. Mol Cell Biol *26*,
739 3282–3294. https://doi.org/10.1128/MCB.26.8.3282-3294.2006.
740 Huang, C.-Y., and Tan, T.-H. (2012). DUSPs, to MAP kinases and beyond. Cell Biosci
741 *2*, 24. https://doi.org/10.1186/2045-3701-2-24.
742 Huang, K., Serria, M.S., Nakabayashi, H., Nishi, S., and Sakai, M. (2000). Molecular
743 cloning and functional characterization of the mouse mafB gene. Gene *242*, 419–426. .
744 Joe, A.W.B., Yi, L., Natarajan, A., Le Grand, F., So, L., Wang, J., Rudnicki, M.A., and
745 Rossi, F.M.V. (2010). Muscle injury activates resident fibro/adipogenic progenitors that
746 facilitate myogenesis. Nat Cell Biol *12*, 153–163. https://doi.org/10.1038/ncb2015.
747 Kassar-Duchossoy, L., Gayraud-Morel, B., Gomès, D., Rocancourt, D., Buckingham,
748 M., Shinin, V., and Tajbakhsh, S. (2004). Mrf4 determines skeletal muscle identity in
749 Myf5:Myod double-mutant mice. Nature *431*, 466–471.
750 https://doi.org/10.1038/nature02876.
751 Kitajima, Y., and Ono, Y. (2018). Visualization of PAX7 protein dynamics in muscle
752 satellite cells in a YFP knock-in-mouse line. Skelet Muscle *8*, 26.
753 https://doi.org/10.1186/s13395-018-0174-x.
754 Kuang, S., Kuroda, K., Le Grand, F., and Rudnicki, M.A. (2007). Asymmetric self-
755 renewal and commitment of satellite stem cells in muscle. Cell *129*, 999–1010.
756 https://doi.org/10.1016/j.cell.2007.03.044.
757 Marti, F., Krause, A., Post, N.H., Lyddane, C., Dupont, B., Sadelain, M., and King, P.D.
758 (2001). Negative-feedback regulation of CD28 costimulation by a novel mitogen-

759 activated protein kinase phosphatase, MKP6. J Immunol *166*, 197–206.
760 https://doi.org/10.4049/jimmunol.166.1.197.
761 Mauro, A. (1961). Satellite cell of skeletal muscle fibers. J Biophys Biochem Cytol *9*,
762 493–495. https://doi.org/10.1083/jcb.9.2.493.
763 Megeney, L.A., Kablar, B., Garrett, K., Anderson, J.E., and Rudnicki, M.A. (1996).
764 MyoD is required for myogenic stem cell function in adult skeletal muscle. Genes Dev.
765 *10*, 1173–1183. https://doi.org/10.1101/gad.10.10.1173.
766 de Morrée, A., van Velthoven, C.T.J., Gan, Q., Salvi, J.S., Klein, J.D.D., Akimenko, I.,
767 Quarta, M., Biressi, S., and Rando, T.A. (2017). Staufen1 inhibits MyoD translation to
768 actively maintain muscle stem cell quiescence. Proc Natl Acad Sci USA *114*, E8996–
769 E9005. https://doi.org/10.1073/pnas.1708725114.
770 Murphy, M.M., Lawson, J.A., Mathew, S.J., Hutcheson, D.A., and Kardon, G. (2011).
771 Satellite cells, connective tissue fibroblasts and their interactions are crucial for muscle
772 regeneration. Development *138*, 3625–3637. https://doi.org/10.1242/dev.064162.
773 Nabeshima, Y., Hanaoka, K., Hayasaka, M., Esuml, E., Li, S., Nonaka, I., and
774 Nabeshima, Y. (1993). Myogenin gene disruption results in perinatal lethality because
775 of severe muscle defect. Nature *364*, 532–535. https://doi.org/10.1038/364532a0.
776 Oki, S., Ohta, T., Shioi, G., Hatanaka, H., Ogasawara, O., Okuda, Y., Kawaji, H.,
777 Nakaki, R., Sese, J., and Meno, C. (2018). ChIP-Atlas: a data-mining suite powered by
778 full integration of public ChIP-seq data. EMBO Rep *19*, e46255.
779 https://doi.org/10.15252/embr.201846255.
780 Olguin, H.C., Yang, Z., Tapscott, S.J., and Olwin, B.B. (2007). Reciprocal inhibition
781 between Pax7 and muscle regulatory factors modulates myogenic cell fate
782 determination. J Cell Biol *177*, 769–779. https://doi.org/10.1083/jcb.200608122.
783 Patterson, K.I., Brummer, T., O'Brien, P.M., and Daly, R.J. (2009). Dual-specificity
784 phosphatases: critical regulators with diverse cellular targets. Biochem J *418*, 475–489.
785 https://doi.org/10.1042/bj20082234.
786 Reiterer, V., Pawłowski, K., Desrochers, G., Pause, A., Sharpe, H.J., and Farhan, H.
787 (2020). The dead phosphatases society: a review of the emerging roles of
788 pseudophosphatases. FEBS J *287*, 4198–4220. https://doi.org/10.1111/febs.15431.
789 Relaix, F., Rocancourt, D., Mansouri, A., and Buckingham, M. (2005). A Pax3/Pax7-
790 dependent population of skeletal muscle progenitor cells. Nature *435*, 948–953.
791 https://doi.org/10.1038/nature03594.
792 Rudnicki, M.A., Braun, T., Hinuma, S., and Jaenisch, R. (1992). Inactivation of MyoD
793 in mice leads to up-regulation of the myogenic HLH gene Myf-5 and results in

794 apparently normal muscle development. Cell *71*, 383–390.
795 https://doi.org/10.1016/0092-8674(92)90508-A.
796 Rudnicki, M.A., Schnegelsberg, P.N.J., Stead, R.H., Braun, T., Arnold, H.-H., and
797 Jaenisch, R. (1993). MyoD or Myf-5 is required for the formation of skeletal muscle.
798 Cell *75*, 1351–1359. https://doi.org/10.1016/0092-8674(93)90621-V.
799 Sabourin, L.A., Girgis-Gabardo, A., Seale, P., Asakura, A., and Rudnicki, M.A. (1999).
800 Reduced Differentiation Potential of Primary MyoD−/− Myogenic Cells Derived from
801 Adult Skeletal Muscle. Journal of Cell Biology *144*, 631–643.
802 https://doi.org/10.1083/jcb.144.4.631.
803 Seale, P., Sabourin, L.A., Girgis-Gabardo, A., Mansouri, A., Gruss, P., and Rudnicki,
804 M.A. (2000). Pax7 Is Required for the Specification of Myogenic Satellite Cells. Cell
805 *102*, 777–786. https://doi.org/10.1016/S0092-8674(00)00066-0.
806 Sénéchal, C., Fujita, R., Jamet, S., Maiga, A., Dort, J., Orfi, Z., Dumont, N.A., Bouvier,
807 M., and Crist, C. (2022). The adhesion G-protein-coupled receptor Gpr116 is essential
808 to maintain the skeletal muscle stem cell pool. Cell Reports *41*, 111645.
809 https://doi.org/10.1016/j.celrep.2022.111645.
810 Tonks, N.K. (2006). Protein tyrosine phosphatases: from genes, to function, to disease.
811 Nat Rev Mol Cell Biol *7*, 833–846. https://doi.org/10.1038/nrm2039.
812 Uezumi, A., Fukada, S., Yamamoto, N., Takeda, S., and Tsuchida, K. (2010).
813 Mesenchymal progenitors distinct from satellite cells contribute to ectopic fat cell
814 formation in skeletal muscle. Nat Cell Biol *12*, 143–152.
815 https://doi.org/10.1038/ncb2014.
816 van Velthoven, C.T.J., and Rando, T.A. (2019). Stem Cell Quiescence: Dynamism,
817 Restraint, and Cellular Idling. Cell Stem Cell *24*, 213–225.
818 https://doi.org/10.1016/j.stem.2019.01.001.
819 Wang, R., Chen, F., Chen, Q., Wan, X., Shi, M., Chen, A.K., Ma, Z., Li, G., Wang, M.,
820 Ying, Y., et al. (2022). MyoD is a 3D genome structure organizer for muscle cell
821 identity. Nat Commun *13*, 205. https://doi.org/10.1038/s41467-021-27865-6.
822 White, J.D., Scaffidi, A., Davies, M., McGeachie, J., Rudnicki, M.A., and Grounds,
823 M.D. (2000). Myotube formation is delayed but not prevented in MyoD-deficient
824 skeletal muscle: studies in regenerating whole muscle grafts of adult mice. J Histochem
825 Cytochem *48*, 1531–1544. https://doi.org/10.1177/002215540004801110.
826 Wood, W.M., Etemad, S., Yamamoto, M., and Goldhamer, D.J. (2013). MyoD-
827 expressing progenitors are essential for skeletal myogenesis and satellite cell
828 development. Developmental Biology *384*, 114–127.
829 https://doi.org/10.1016/j.ydbio.2013.09.012.

Yablonka-Reuveni, Z., Rudnicki, M.A., Rivera, A.J., Primig, M., Anderson, J.E., and Natanson, P. (1999). The Transition from Proliferation to Differentiation Is Delayed in Satellite Cells from Mice Lacking MyoD. Developmental Biology *210*, 440–455. https://doi.org/10.1006/dbio.1999.9284.

Yamamoto, M., Legendre, N.P., Biswas, A.A., Lawton, A., Yamamoto, S., Tajbakhsh, S., Kardon, G., and Goldhamer, D.J. (2018). Loss of MyoD and Myf5 in Skeletal Muscle Stem Cells Results in Altered Myogenic Programming and Failed Regeneration. Stem Cell Reports *10*, 956–969. https://doi.org/10.1016/j.stemcr.2018.01.027.

Zammit, P.S., Partridge, T.A., and Yablonka-Reuveni, Z. (2006). The Skeletal Muscle Satellite Cell: The Stem Cell That Came in From the Cold. J Histochem Cytochem. *54*, 1177–1191. https://doi.org/10.1369/jhc.6R6995.2006.

Zismanov, V., Chichkov, V., Colangelo, V., Jamet, S., Wang, S., Syme, A., Koromilas, A.E., and Crist, C. (2016). Phosphorylation of eIF2α Is a Translational Control Mechanism Regulating Muscle Stem Cell Quiescence and Self-Renewal. Cell Stem Cell *18*, 79–90. https://doi.org/10.1016/j.stem.2015.09.020.

Zou, Z., Ohta, T., Miura, F., and Oki, S. (2022). ChIP-Atlas 2021 update: a data-mining suite for exploring epigenomic landscapes by fully integrating ChIP-seq, ATAC-seq and Bisulfite-seq data. Nucleic Acids Res *50*, W175–W182. https://doi.org/10.1093/nar/gkac199.

KEY RESOURCES TABLE

REAGENT or RESOURCE	SOURCE	IDENTIFIER
Antibodies		
anti-PAX7	Santa Cruz	Cat# sc-81648; RRID: AB_2159836
anti-MYOD	Santa Cruz	Cat# sc-377460, RRID: AB_2813894
anti-MYOGENIN	abcam	Cat# ab124800, RRID: AB_10971849
Anti-KI67	Invitrogen	Cat# MA5-14520, RRID:AB_10979488
Anti-LAMININ2 ALPHA	abcam	Cat# ab11576, RRID:AB_298180
Anti-MYH1E	DSHB	MF20, RRID:AB_2147781
Alexa Fluor 488 goat anti-mouse IgG1	Thermo Fisher Scientific	Cat# A-21121, RRID: AB_2535764
Alexa Fluor 555 goat anti-mouse IgG1	Thermo Fisher Scientific	Cat# A-21127, RRID:AB_2535769
Alexa Fluor 546 goat anti-rabbit IgG	Thermo Fisher Scientific	Cat# A-11010, RRID: AB_2534077
Alexa Fluor 546 goat anti-mouse IgG2b	Thermo Fisher Scientific	Cat# A-21143, RRID:AB_2535779
Alexa Fluor 633 goat anti-rabbit IgG	Thermo Fisher Scientific	Cat# A-21070, RRID:AB_2535731
Alexa Flour 647 donkey anti-rat IgG	abcam	Cat# ab150155, RRID:AB_2813835
Satellite Cell Isolation Kit	Miltenyi Biotec	Cat# 130-104-268
anti-mouse integrin α-7 MicroBeads	Miltenyi Biotec	Cat# 130-104-261
Bacterial and Virus Strains		
pAd-CMV-EDFP	This study	N/A
pAd-CMV-Dusp13-IRES-EDFP	This study	N/A
pAd-CMV-Dusp13_Mut-IRES-EDFP	This study	N/A
Chemicals, Peptides, and Recombinant Proteins		
DMEM	Thermo Fisher Scientific	Cat# 11965-092
F12	Thermo Fisher Scientific	Cat# 11765-054
Collagenase D	Roche	Cat# 11088866001
D-PBS (-)	FUJIFILM	Cat# 045-29795
OPTI-MEM	Thermo Fisher Scientific	Cat# 31985062
M.O.M. Blocking Reagent	Vector	Cat# MKB-2213-1
Cardiotoxin	LATOXIAN	Cat# 56574-47-1
TRIzol	Thermo Fisher Scientific	Cat# 15596018
Gelatin from porcine skin	MERK	Cat# G1890

Ultroser G	PALL	Cat# 15950-017
Fetal bovine serum	Thermo Fisher Scientific	Cat# 10270-106
Horse serum	Thermo Fisher Scientific	Cat# 26050088
SsoAdvanced™ Universal SYBR Green Supermix	Bio-Rad	Cat# 1725271
4% Paraformaldehyde Fixative	MUTO PURE CHEMICALS CO., LTD.	Cat# 33111
FuGENE 6 Transfection	Promega	Cat# E2692
PrimeSTAR Max DNA	TAKARA BIO Inc.	Cat# R045A
PrimeSTAR Mutagenesis Basal Kit	TAKARA BIO Inc.	Cat#R046A
Normal Goat Serum	Vector	Cat# S-1000
VECTASHIELD Vibrance Antifade Mounting Medium with DAPI	Vector	Cat# H-1800
Glycerol Gelatin	Sigma-Aldrich	Cat# GG1-15ML
Mayer's Hematoxylin Solution	FUJIFILM Wako Pure Chemical Corporation	Cat# 131-09665
Bovine Serum Albumin	Sigma-Aldrich	Cat# A7906
Tragacanth Gum, Powder	FUJIFILM Wako Pure Chemical Corporation	Cat# 200-02245
DPX. Neutral mounting medium	Sigma-Aldrich	Cat# 317616
RNase-free Water, non DEPC	Biodynamics Laboratory Inc.	Cat# DR127
Ethanol (99.5)	FUJIFILM Wako Pure Chemical Corporation	Cat# 057-00456
Ethanol (99)	FUJIFILM Wako Pure Chemical Corporation	Cat# 056-06967
Xylene	FUJIFILM Wako Pure Chemical Corporation	Cat# 242-00087
Acetone	FUJIFILM Wako Pure Chemical Corporation	Cat# 016-00346
Critical Commercial Assays		
Satellite cell isolation Kit, mouse	Miltenyi Biotec	Cat# 130-104-268
ReverTra Ace™ qPCR RT Master Mix with gDNA Remover	TOYOBO	Cat# FSQ-301

Wizard Plus SV Minipreps DNA Purification System	Promega	Cat# A1460
QIAquick PCR Purification Kit	QIAGEN	Cat# 28104
In-Fusion® HD Cloning Kit	TAKARA BIO Inc.	Cat# Z9649N
QuikChange Site-Directed Mutagenesis Kit	Agilent	Cat# 200519
Dual-Luciferase® Reporter Assay System	Promega	Cat# E1910
Deposited Data		
Single RNA-seq data	This paper	Accession number: GSE250228
Experimental Models: Cell Lines		
AAVpro 293T Cell Line	Takara Bio	Cat# 632273
Experimental Models: Organisms/Strains		
Mouse: C57BL/6J	The Jackson Laboratory	RRID:IMSR_JAX:000664
Mouse: Dusp13 KO	This paper	N/A
Mouse: Dusp27 KO	This paper	N/A
Mouse: Pax7-YFP	Kitajima et al.	PMID: 30139390
Mouse: *C57BL/6J-Myod1*$^{em1(tdTomato)Utr}$ *(MyoD*^{KI}*)*	Fujita et al.	PMID: 37250337
Oligonucleotides		
See Table S1 for genotyping primers	This paper	N/A
See Table S1 for RT-qPCR primers	This paper	N/A
See Table S1 for cloning primers	This paper	N/A
Recombinant DNA		
pGL4-Dusp13	This study	N/A
pGL4-Dusp27	This study	N/A
pAAV-MyoD	This study	N/A
Software and Algorithms		
ImageJ	NIH	https://imagej.net/software/fiji/
Illustrator	Adobe	N/A
Photoshop	Adobe	N/A
Chromium Next GEN Single Cell 3'Reagent Kits v3.1	10× Genomics	Cat# 1000268
Chromium controller	10× Genomics	https://www.10xgenomics.com/
NovaSeq 6000	Ilumina	https://jp.illumina.com/
MEME FIMO v5.5.0	Grant et al.[51]	RRID:SCR_001783
Prism v10	GraphPad	https://www.graphpad.com/
Other		
Thermal Cycler Dice® Real Time System Single	Takara Bio	Cat# TP850

GloMax® 20/20 Luminometer	Promega	Cat# E5311
NanoDrop™ 2000/2000c	Thermo-Fisher Scientific	Cat# ND-2000

849 **Figures**

Figure 1 (Hayashi et al.)

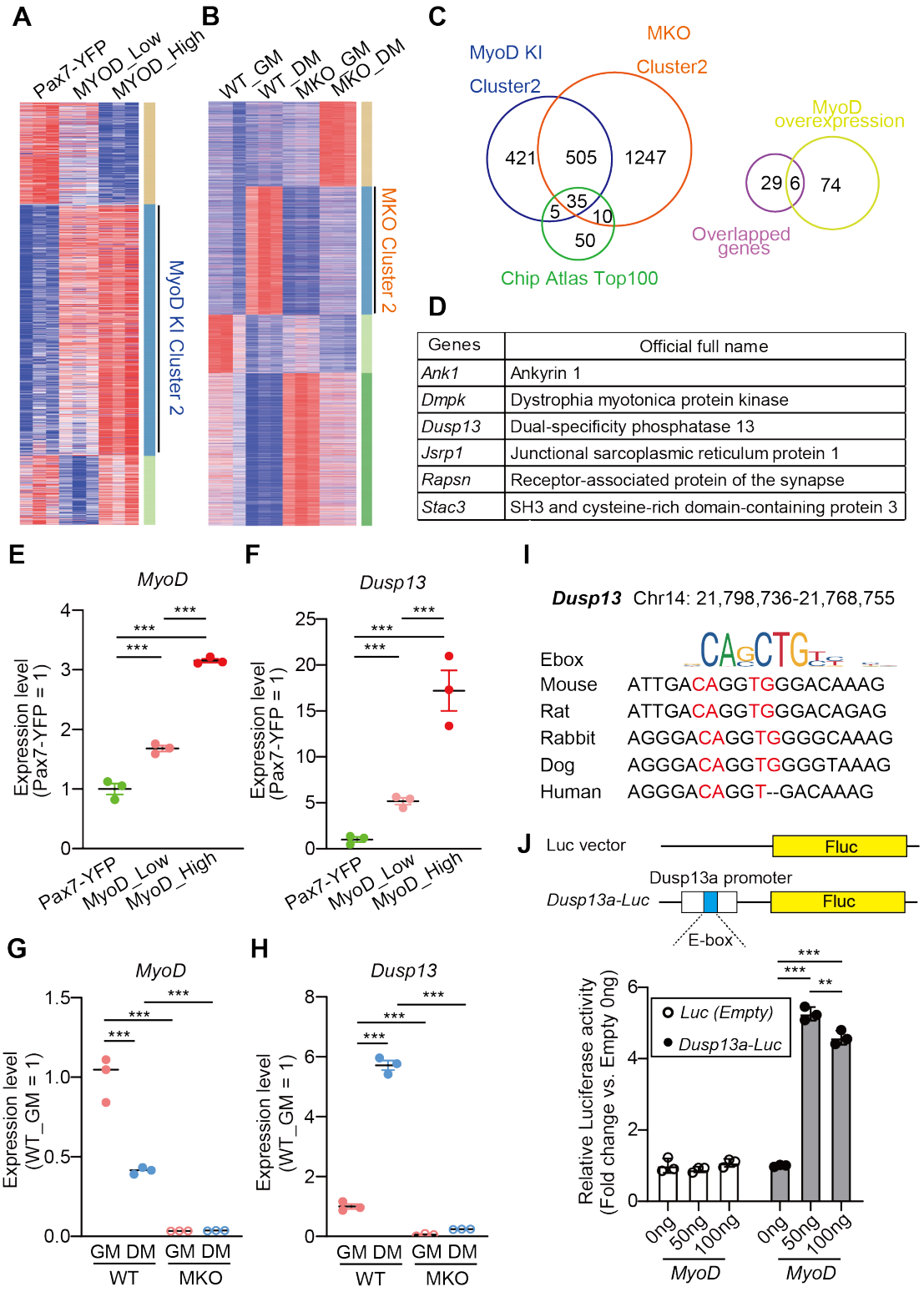

850

851 **Figure 1. *Dusp13* is a novel target regulated by MyoD**

852 **(A)** Clustering heatmap showing differentially expressed genes in RNA-seq data from Pax7-YFP
853 (Quiescent MuSCs; QSCs), MyoD-low (MyoD-tdTomato low), and MyoD-high (MyoD-tdTomato
854 high) (n = 3 per group).
855 **(B)** Clustering heatmap of differentially expressed genes in RNA-seq between wild-type (WT**)** growth
856 medium (GM) (WT_GM), *MyoD* knock-out GM (MKO_GM), WT differentiation medium (WT_DM),
857 and MKO_DM (n = 3 per group).
858 **(C)** Venn diagrams of indicated clusters from (**A, B)** and ChIP atlas top 100 genes potentially regulated
859 by *MyoD* (Left). Venn diagrams of overlapped 35 genes (left) and 80 genes upregulated by *MyoD*
860 overexpression in MEFs (Right).
861 **(D)** The list of six genes from (**C**).
862 **(E, F)** Gene expression of *MyoD* (**E**) or *Dusp13* (**F**) analyzed by RNA-seq in the Pax7-YFP, MyoD-
863 low, and MyoD-high MuSCs (n = 3 per group).
864 **(G, H)** Gene expression of *MyoD* (**G**) or *Dusp13* (**H**) analyzed by RNA-seq in the WT_GM, WT_DM,
865 MKO_GM, and MKO_DM (n = 3 per group).
866 **(I)** E box-like sequences in the promoter region of *Dusp13* in mammalian species.
867 **(J)** Luciferase reporter constructs of *Dusp13* upstream region (−150 to +50) containing an E box-like
868 sequence (Top). Relative *Dusp13*-luciferase reporter activities in HEK293T cells overexpressing
869 *MyoD* (Bottom) (n = 3 per group).
870
871 All data are represented as the mean ± standard error of the mean (SEM)
872 P values calculated using edge R **(E, F)** (FDR-corrected), DEseq2 **(G, H)** (FDR-corrected), or Tukey's
873 test **(J)**; **P < 0.01, ***P < 0.001, n.s., not significant.
874

Figure 2 (Hayashi et al.)

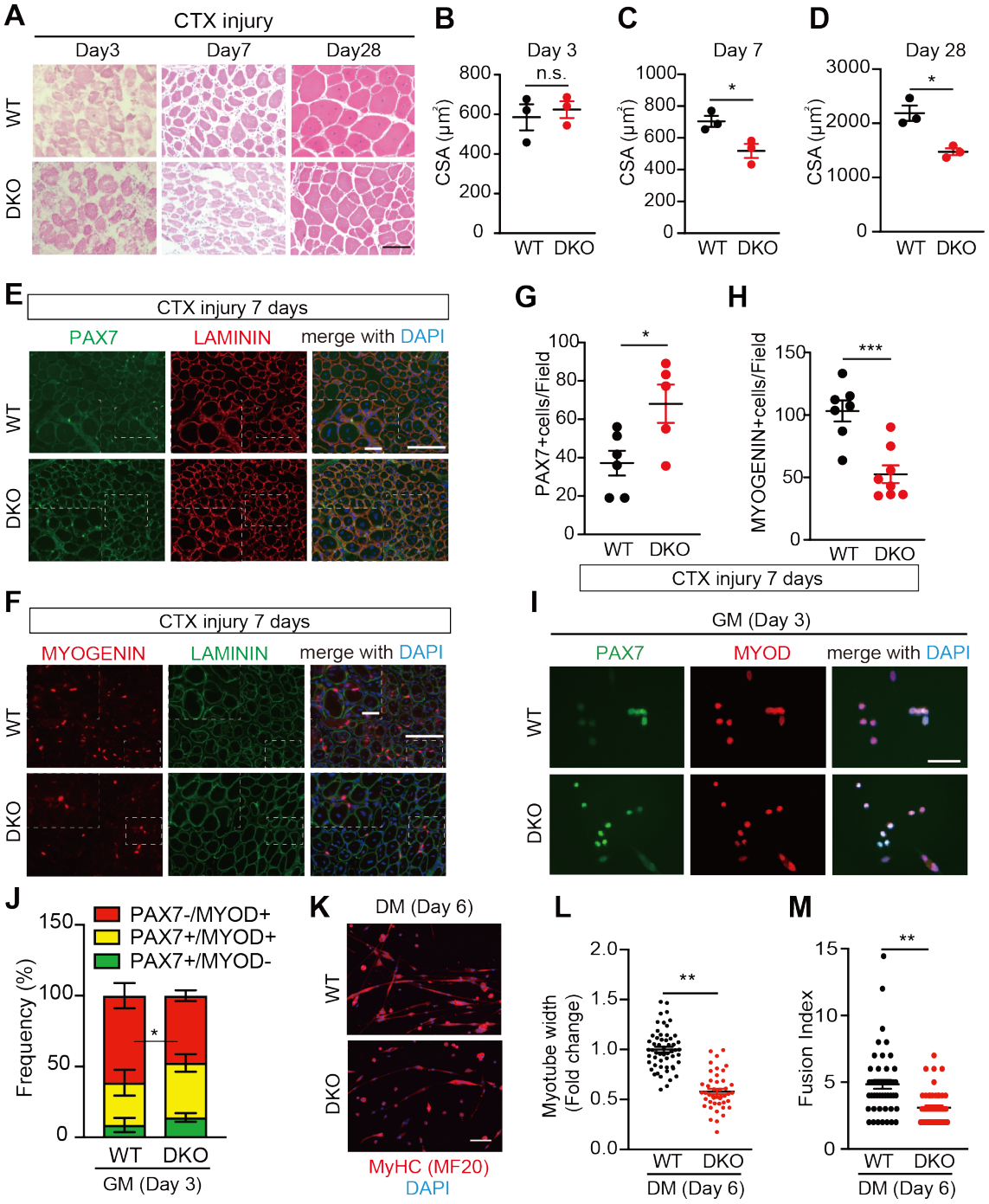

Figure 2. Loss of both *Dusp13* and *Dusp27* impairs muscle regeneration after acute muscle injury.

(A) Hematoxylin and eosin (H&E) staining of tibialis anterior (TA) muscle cross-sections of male *Dusp13* and *Dusp27* double knock-out (DKO) (n = 3) and WT (n = 3) mice at 12–15 weeks of age, 3, 7, and 28 days post-cardiotoxin (CTX) injury. Scale bar: 100 μm.

882 **(B–D)** Cross-sectional area (CSA) of damaged TA muscles at indicated time points.
883 **(E, F)** Immunofluorescence of PAX7 (**E**) or MYOGENIN (**F**) with LAMININ on sections of TA
884 muscles from WT and DKO mice, 7 days post-CTX injury. Nuclei are stained with DAPI. Scale bar:
885 100 µm. The area in white dotted boxes is shown at a higher magnification. Scale bar: 25 µm.
886 **(G, H)** Average number of PAX7 (+) or MYOGENIN (+) nuclei in **(E)** and **(F)** are quantified (n =
887 5–8 independent experiments).
888 **(I)** Immunofluorescence of PAX7 and MYOD on cultured MuSCs from WT and DKO mice. Nuclei
889 are stained with DAPI. Scale bar: 100 µm.
890 **(J)** Quantification of the proportion of MuSCs undergoing self-renewal (PAX7 (+), MYOD (-)),
891 activation (PAX7 (+), MYOD (+)), and differentiation [PAX7 (+), MYOD (-)] in (**I**). (n = 6
892 independent experiments)
893 **(K)** Immunofluorescence with an antibody against myosin heavy chain (MyHC) on MuSCs
894 differentiated for six days in DM. Nuclei are stained with DAPI. Scale bar: 100 µm.
895 **(L, M)** Myotube width **(L)** and Fusion index (numbers of myonuclei per MyHC (+) myotube) **(M)**
896 in **(K)** are quantified (WT, n = 50**;** DKO, n = 53).
897
898 All data are represented as the mean ± standard error of the mean (SEM)
899 P values calculated using Student's t-test; *P < 0.05, **P < 0.01, ***P < 0.001, n.s., not significant.
900

Figure 3 (Hayashi et al.)

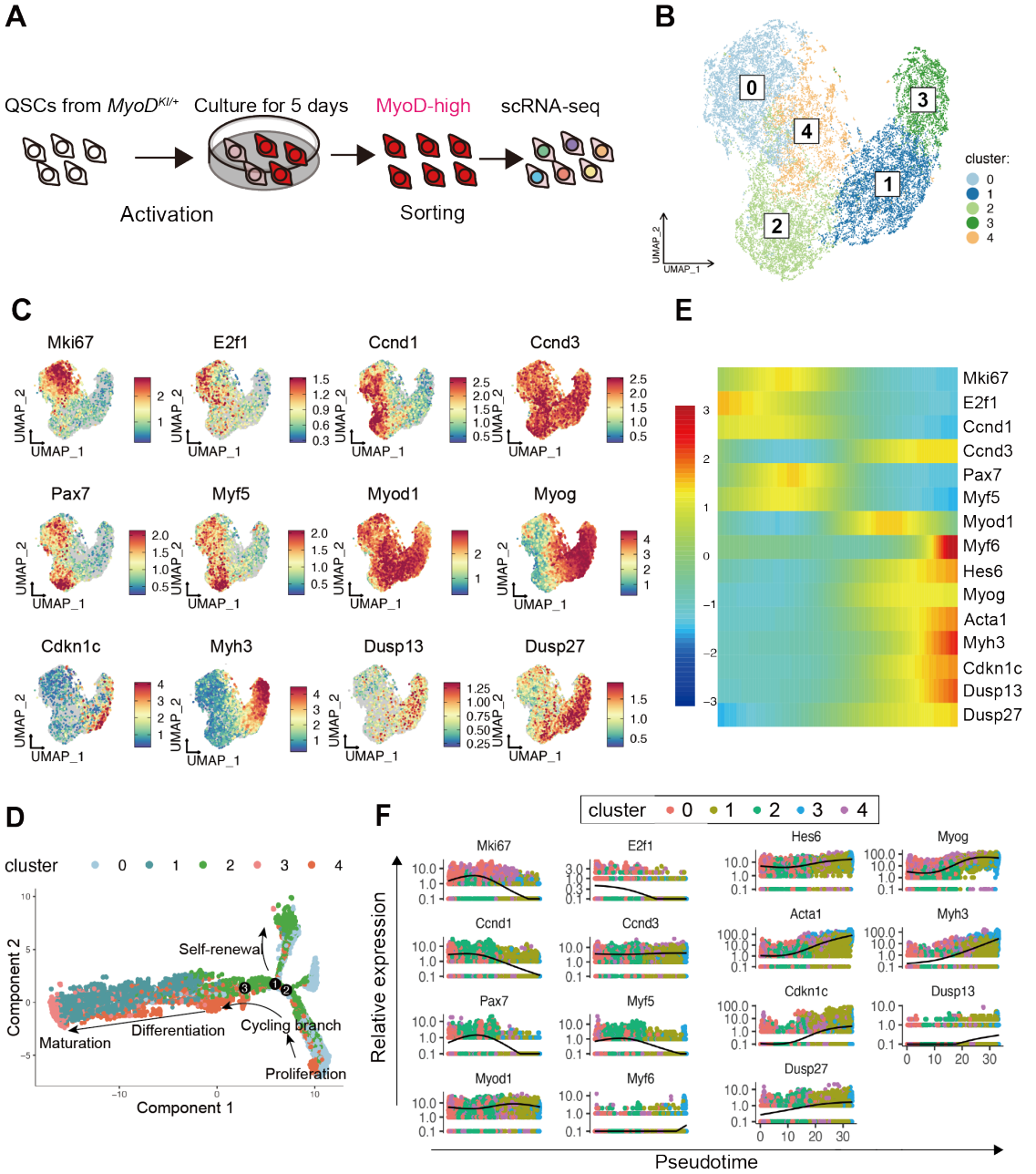

Figure 3. Single-cell RNA-sequencing analysis of MyoD-high MuSCs from MyoD-KI mice reveals *Dusp13* and *Dusp27* expression in the mature stage of MuSCs.

(A) Schematic diagram illustrating the scRNA-seq analysis of MyoD-high MuSCs from MyoD-KI mice.

(B) Transcriptomic atlas and clustering of the subset of MyoD-high MuSCs from MyoD-KI mice.

(C) Single-cell expression pattern of the target genes.

(D) Pseudotime analysis performed using the Monocle package. The plot depicts the hierarchy of MyoD-high MuSCs in the pseudotime trajectory.

910 **(E)** A heatmap showing the expression of representative genes in the pseudotime analysis. Each
911 column represents a cell, and each row represents a gene.
912 **(F)** Pseudotime-ordered single-cell expression of representative genes.

Figure 4 (Hayashi et al.)

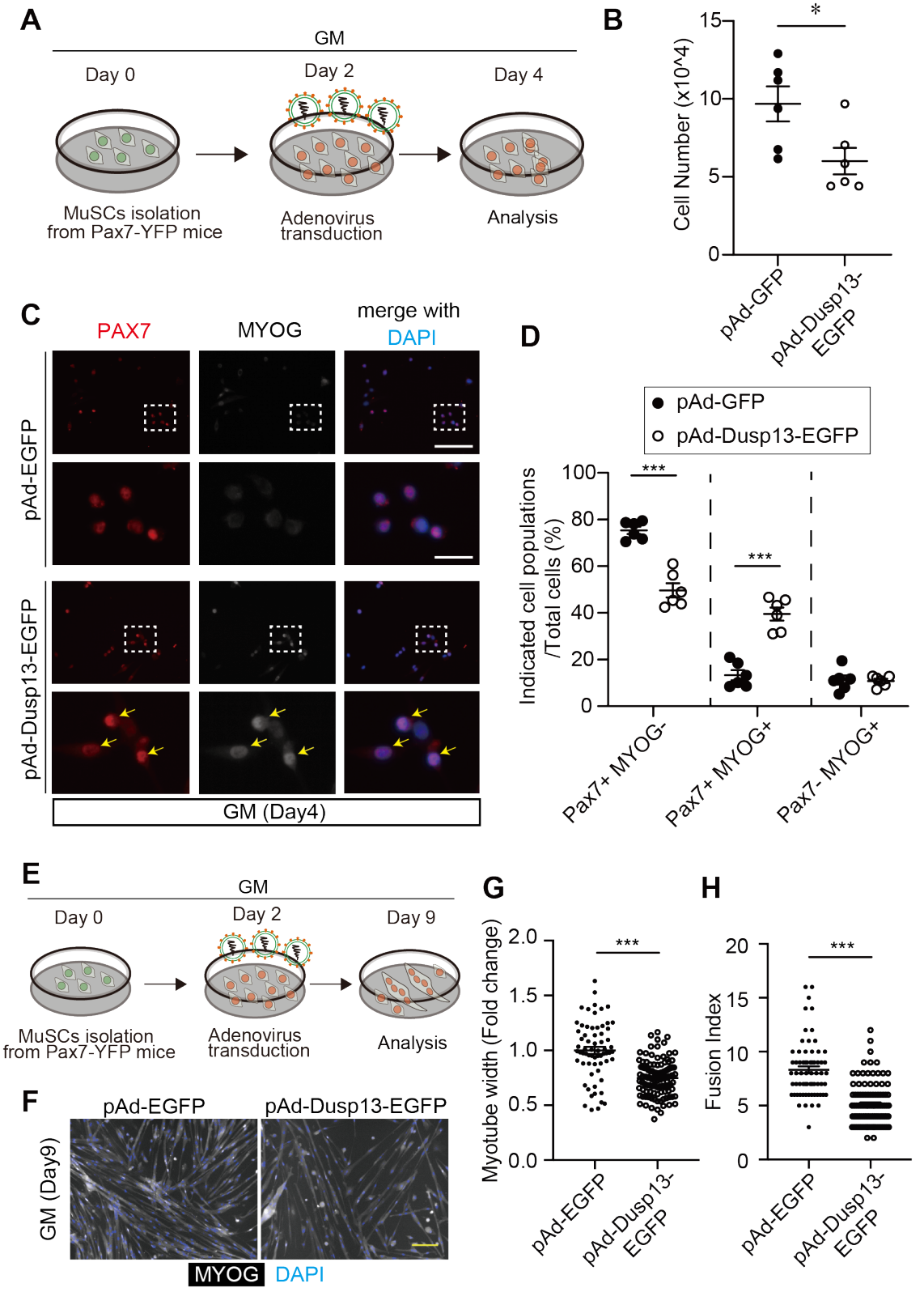

913

914 **Figure 4. Overexpression of *Dusp13* induces precocious muscle differentiation independent of**
915 **phosphatase activity.**
916
917 **(A)** Schematic diagram illustrating adenovirus infection into MuSCs from Pax7-YFP mice on day 4
918 of growth medium (GM) culture.
919 **(B)** Number of cultured MuSCs after transduction with adenovirus vectors overexpressing GFP (pAd-
920 EGFP) or Dusp13 (pAd-Dusp13-EGFP).
921 **(C)** Immunofluorescence staining of PAX7 and MYOGENIN in cultured MuSCs after transduction
922 with adenovirus vectors overexpressing GFP (pAd-EGFP) or Dusp13 (pAd-Dusp13-EGFP) on GM
923 day 4. Nuclei are stained with DAPI. The yellow arrow indicates PAX7 (+)/MYOGENIN (+) cells. (n
924 = 6 per group). Scale bar: 100 μm (Upper); 25 μm (Bottom).
925 **(D)** The proportion of each population in (**C**).
926 **(E)** Schematic diagram illustrating adenovirus infection into MuSCs from Pax7-YFP mice on GM day
927 9.
928 **(F)** Immunofluorescence staining of MYOGENIN in cultured MuSCs after transduction with
929 adenovirus vectors overexpressing GFP (pAd-EGFP) or Dusp13 (pAd-Dusp13-EGFP) on GM day 9.
930 Nuclei are stained with DAPI. Scale bar: 100 μm
931 **(G, H)** Myotube width **(G)** and Fusion index (numbers of myonuclei per myotube) **(H)** in **(F)** are
932 quantified (WT, n = 66, DKO, n = 104)
933 All data are represented as the mean ± standard error of the mean (SEM)
934 P values calculated using Student's t-test; *P < 0.05, **P < 0.01, ***P < 0.001, n.s., not significant.

Supplementary Data

Supplementary Figure 1 (Hayashi et al.)

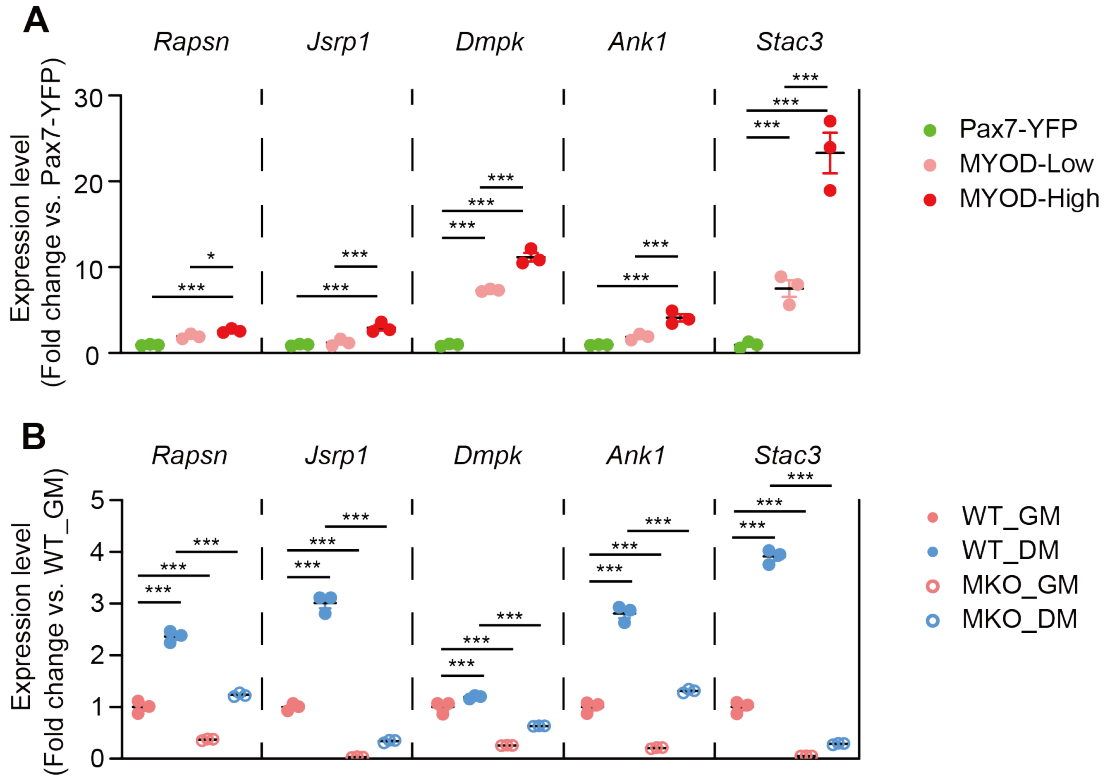

Figure S1. Expression changes of candidate genes that are potentially MyoD-regulated.

(A) Gene expression of *Rapsn*, *Jsrp1*, *Dmpk*, *Ank1*, and *Stac3* in RNA-seq data from Pax7-YFP (Quiescent MuSCs; QSCs), MyoD-low (MyoD-tdTomato low), and MyoD-high (MyoD-tdTomato high) (n = 3 per group).

(B) Gene expression of *Rapsn*, *Jsrp1*, *Dmpk*, *Ank1*, and *Stac3* in RNA-seq between wild-type (WT)_growth medium (GM) (WT_GM), *MyoD* knock-out_GM (MKO_GM), WT_differentiation medium (WT_DM), and MKO_DM (n = 3 per group).

All data are represented as the mean ± standard error of the mean (SEM)

P values calculated using edge R **(A)** (FDR-corrected), DEseq2 **(B)** (FDR-corrected); *P < 0.05, ***P < 0.001 among all groups.

Supplementary Figure 2 (Hayashi et al.)

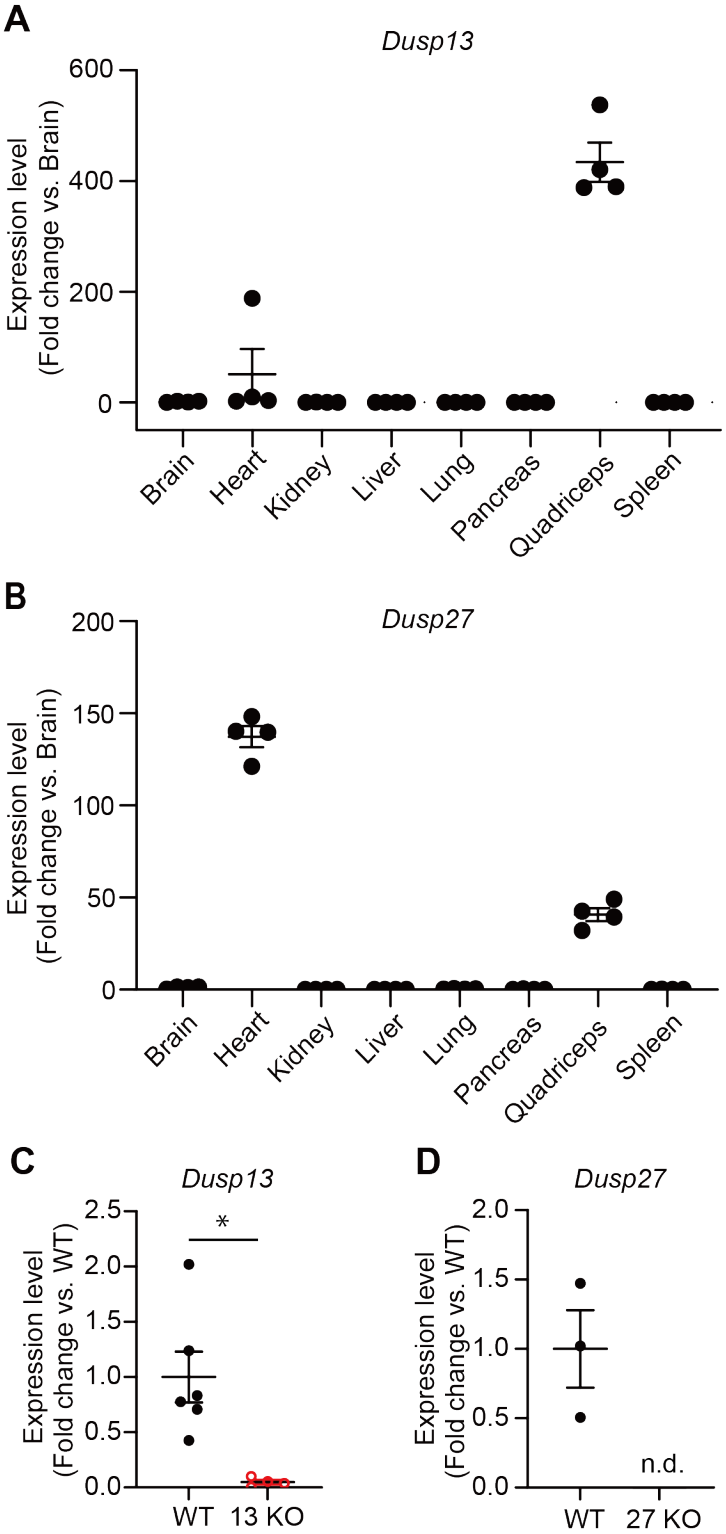

Figure S2. Expression pattern of *Dusp13/Dusp27* in a collection of tissues.

(A, B) qPCR analysis of *Dusp13* (A) and *Dusp27* (B) mRNA levels in the tissues (brain, heart, kidney, liver, lung, pancreas, muscle, and spleen) of WT mice at 13–14 weeks (n = 4 per tissue).

(C) qPCR analysis of *Dusp13* mRNA levels in the gastrocnemius muscles of WT and *Dusp13* KO (13 KO) mice at 8–12 weeks (n = 4–6 independent experiments).

(D) qPCR analysis of *Dusp27* mRNA levels in the gastrocnemius muscles of WT and *Dusp27* KO (27 KO) mice at 8–12 weeks (n = 3 per group).

All data are represented as the mean ± standard error of the mean (SEM)

P values calculated using Student's t-test; *P < 0.05, n.d., not detected.

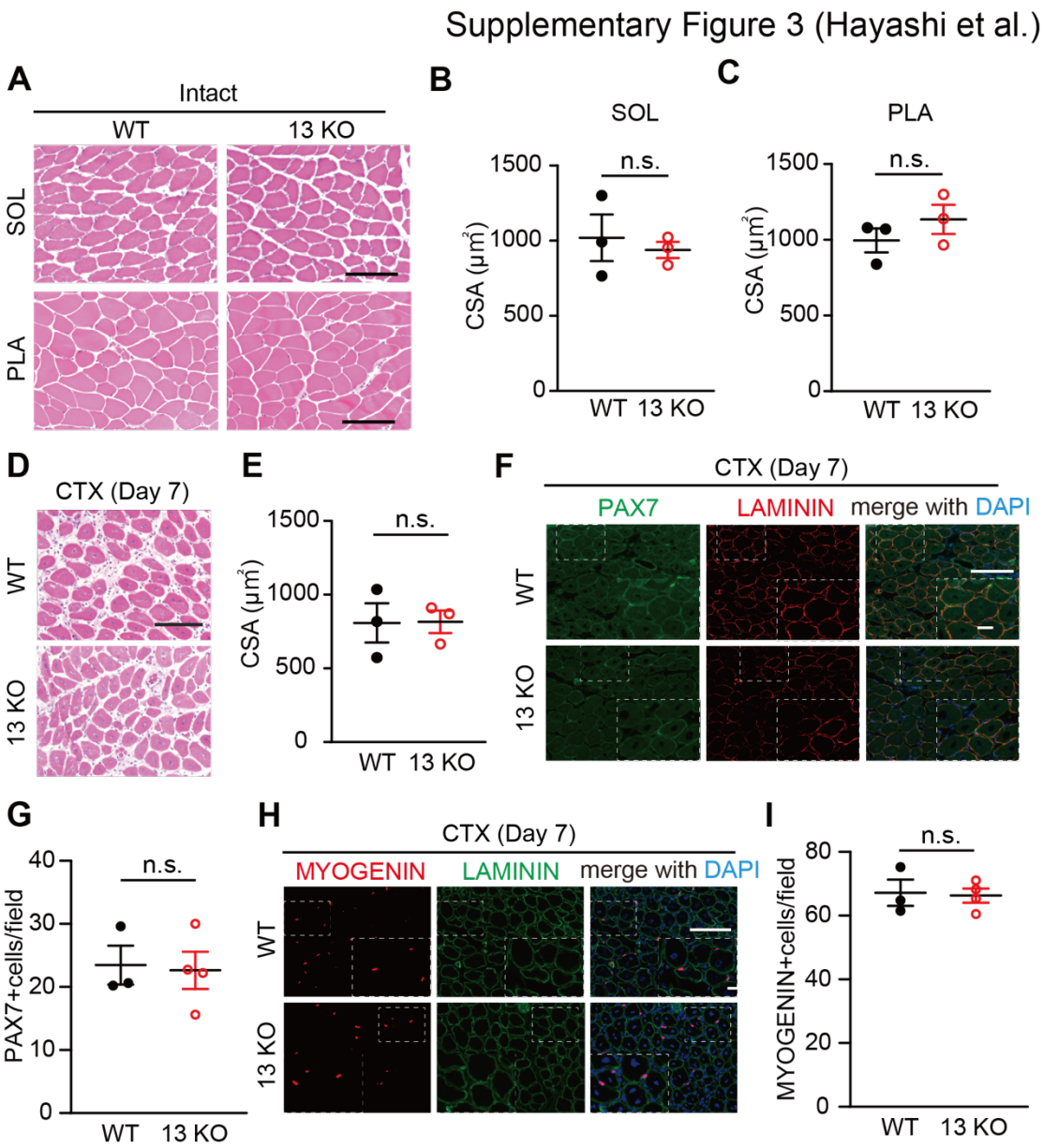

Figure S3. Absence of skeletal muscle phenotype in *Dusp13* knock-out (13 KO) mice during development and regeneration.

(A) Hematoxylin and eosin (H&E) staining of Soleus (SOL) and Plantaris (PLA) muscle cross-sections of male *Dusp13* knock-out (13 KO) and WT mice at 10 weeks. Scale bar: 100 μm.

(B, C) Cross-sectional area (CSA) of SOL (B) or PLA (C) (n = 3 per group).

(D) H&E staining of tibialis anterior (TA) muscle cross-sections of male 13 KO and WT mice at 12 weeks, 7 days post cardiotoxin (CTX) injury. Scale bar: 100 μm.

(E) CSA of damaged TA muscles (n = 3 per group).

(F) Immunofluorescence of PAX7 with LAMININ on sections of TA muscles from WT and *Dusp13* KO mice, 7 days post-CTX injury. Nuclei are stained with DAPI. Scale bar: 100 μm. The area in the white dotted boxes is shown at a higher magnification. Scale bar: 25 μm.

(G) Average number of PAX7 (+) nuclei in **(F)** are quantified (n = 3–4 independent experiments).

(H) Immunofluorescence of MYOGENIN with LAMININ on sections of TA muscle from WT and 13 KO mice, 7 days post-CTX injury. Nuclei are stained with DAPI. Scale bar: 100 μm. The area in the white dotted boxes is shown at a higher magnification. Scale bar: 25 μm.

(I) Average number of MYOGENIN (+) nuclei in **(H)** are quantified (n = 3–4 independent experiments).

All data are represented as the mean ± standard error of the mean (SEM)

P values calculated using Student's t-test; n.s., not significant.

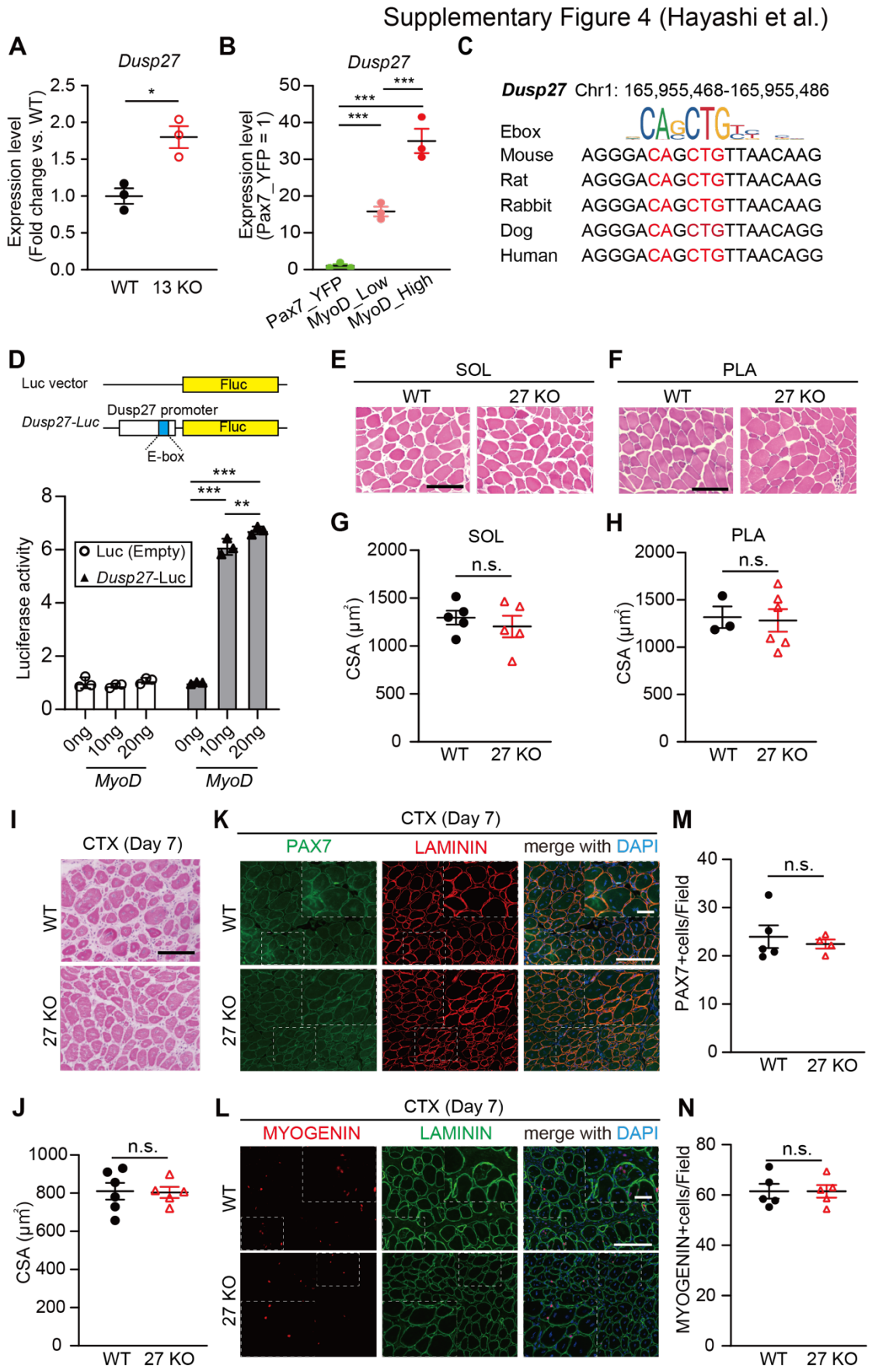

Figure S4. ***Dusp27*** **KO mice exhibit comparable muscle development and regeneration to WT mice.**

(A) qPCR analysis of *Dusp27* mRNA levels in gastrocnemius muscles of WT and 13 KO mice at 12 weeks (n = 3 per group).

(B) Gene expression of *Dusp27* in RNA-seq data from Pax7-YFP, MYOD-low, and MYOD-high (n = 3 per group).

(C) Ebox-like sequences in the promoter region of *Dusp27* in mammalian species.

(D) Luciferase reporter constructs of *Dusp27* upstream region (−1,000 to +200) containing an Ebox-like sequence (Top). Relative *Dusp27*-luciferase reporter activities in HEK293T cells overexpressing MyoD (Bottom) (n = 3 per group).

(E, F) H&E staining of SOL and PLA muscle cross-sections. Scale bar: 100 μm.

(G, H) CSA of SOL **(G)** or PLA **(H)** muscles of male *Dusp27* KO (27 KO) and WT (n = 3–6 independent experiments) mice at 12 weeks.

(I) H&E staining of TA muscle cross-sections of male 27 KO and WT mice at 12 weeks (n = 5–6 independent experiments), 7 days post-cardiotoxin injury. Scale bar: 100 μm.

(J) CSA of damaged TA muscles.

(K, L) Immunofluorescence of PAX7 **(K)** or MYOGENIN **(L)** with LAMININ on sections of TA muscles from WT and 27 KO mice, 7 days post-CTX injury. Nuclei are stained with DAPI. Scale bar: 100 μm. The area in the white dotted boxes is shown at a higher magnification. Scale bar: 25 μm.

(M, N) Average number of PAX7 (+) or MYOGENIN (+) nuclei in (M) and (N) are quantified (n = 5–8 independent experiments).

All data are represented as the mean ± standard error of the mean (SEM)

P values calculated using Student's t-test, and edge R; *P < 0.05, **P < 0.01, ***P < 0.001, n.s., not significant.

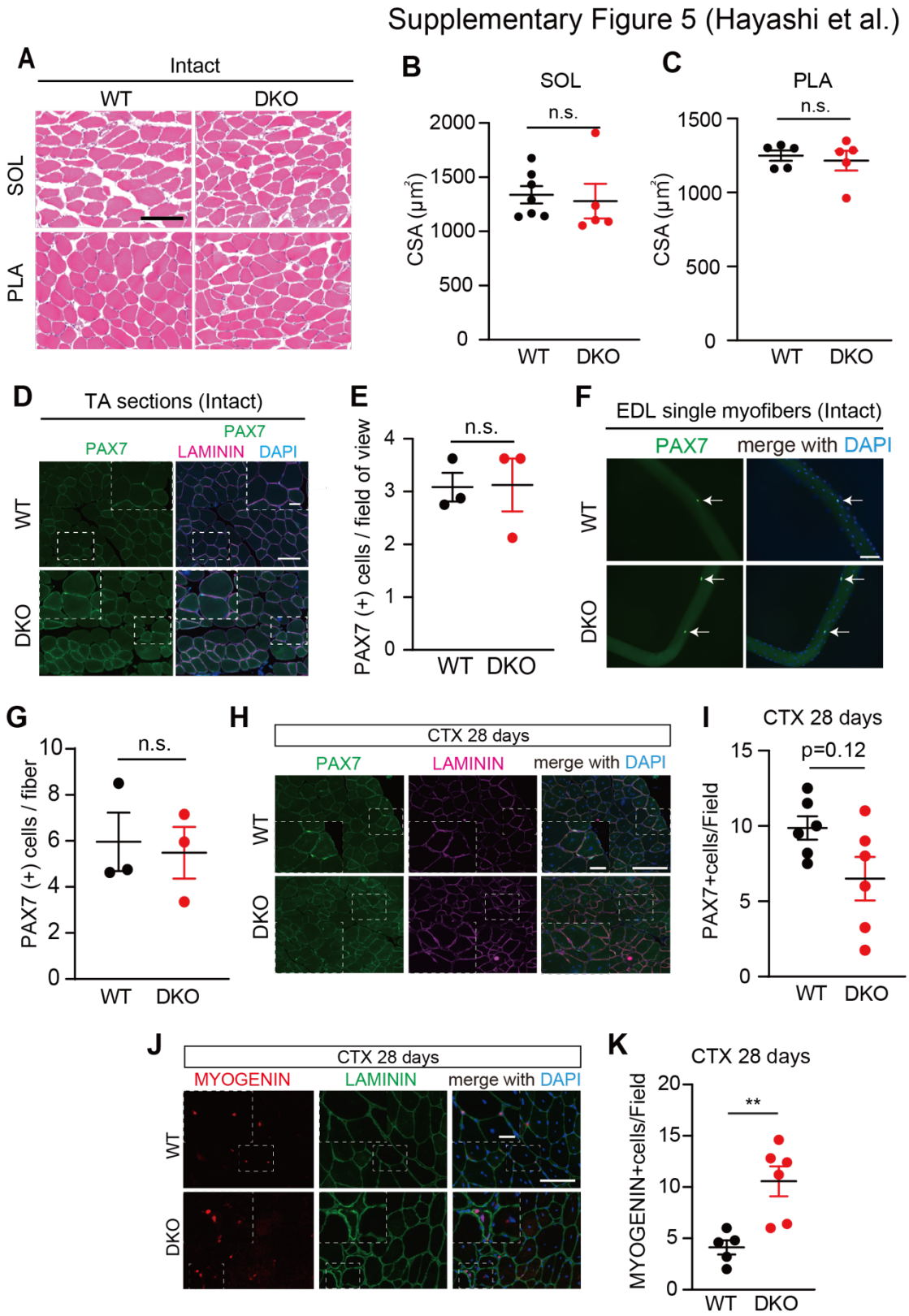

Figure S5. Comparative analysis of intact muscles in *Dusp13*:*Dusp27* DKO mice and WT mice.

(A) H&E staining of SOL and PLA muscle cross-sections. Scale bar: 100 μm.

(B, C) CSA of SOL **(B)** or PLA **(C)** muscles of male *Dusp13*:*Dusp27* double knock-out (DKO) and WT mice at 13 weeks (n = 5–7 independent experiments).

(D) Immunoflurescence of PAX7 and LAMININ in intact TA muscles. Scale bar: 100 μm. The area in the white dotted boxes is shown at a higher magnification. Scale bar: 25 μm. **(E)** Average number of PAX7 (+) nuclei in DAPI (+) in **(D)**.

(F) Immunofluorescence of PAX7 on freshly isolated single extensor digitorum longus (EDL) myofibers from DKO and WT mice at 13 weeks (n = 3 per group). Nuclei stained with DAPI. White arrows indicate PAX7 (+) cells on EDL myofibers. Scale bar: 100 μm.

(G) Number of PAX7 (+) cells EDL myofibers in **(F)**.

(H) Immunofluorescence of PAX7 with LAMININ on sections of TA muscles from WT and DKO mice, 28 days post-CTX injury. Nuclei are stained with DAPI. Scale bar: 100 μm. The area in the white dotted boxes is shown at a higher magnification. Scale bar: 25 μm.

(I) Average number of PAX7 (+) nuclei in **(H)** are quantified (n = 6 per group).

(J) Immunofluorescence of MYOGENIN with LAMININ on sections of TA muscles from WT and DKO mice, 28 days post-CTX injury. Nuclei are stained with DAPI. Scale bar: 100 μm. The area in the white dotted boxes is shown at a higher magnification. Scale bar: 25 μm.

(K) Average number of MYOGENIN (+) nuclei in **(J)** are quantified (n = 4–6 independent experiments).

All data are represented as the mean ± standard error of the mean (SEM)

P values calculated using Student's t-test; **P < 0.01, n.s., not significant.

Supplementary Figure 6 (Hayashi et al.)

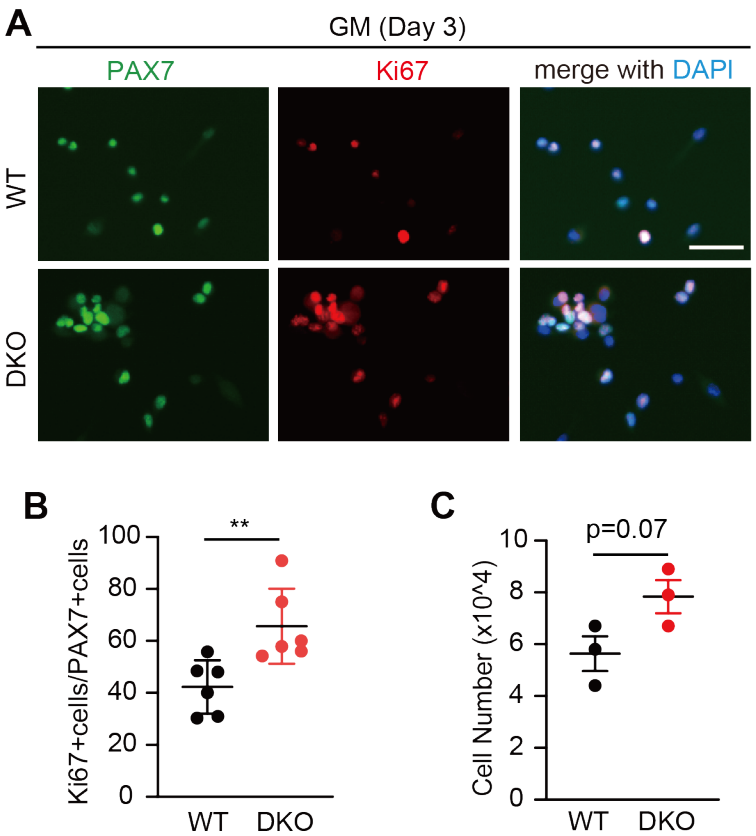

Figure S6. MuSCs derived from *Dusp13*:*Dusp27* DKO mice stay in the proliferation stage.

(A) Immunofluorescence of PAX7 and Ki67 on MuSCs cultured for three days in a growth medium (GM).

(B) Average number of Ki67 (+) nuclei in PAX7 (+) in **(A)** are quantified (n = 6 per group).

(C) Cell numbers of MuSCs derived from WT or DKO at GM day 4 (n = 3 per group).

All data are represented as the mean ± standard error of the mean (SEM)

P values calculated using Student's t-test; **P < 0.01.

Supplementary Figure 7 (Hayashi et al.)

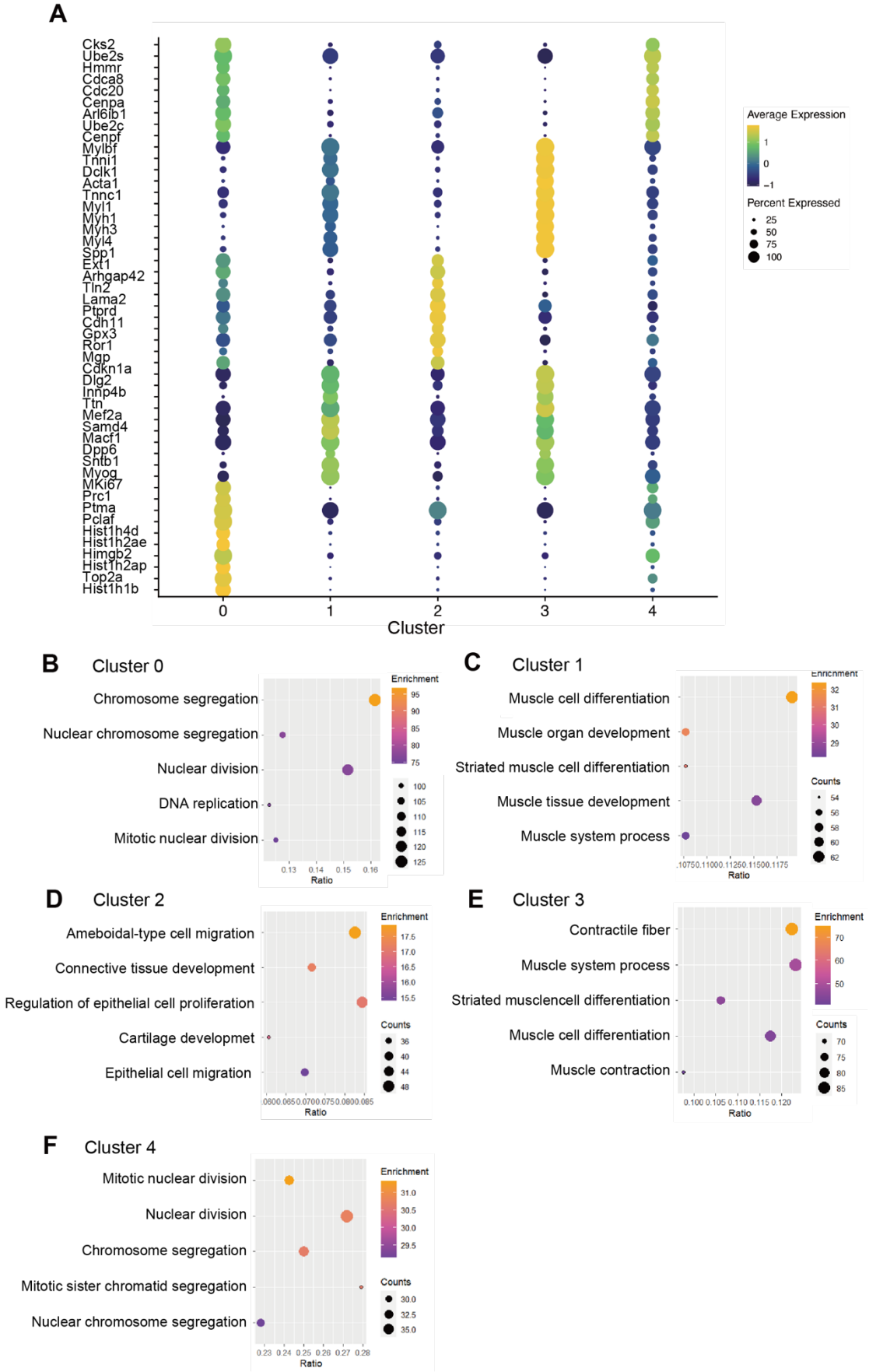

Figure S7. Pathway analysis in single-cell RNA-sequencing data of MYOD-high MuSCs from MyoD-KI mice.

(A) Dot plot representing the expression of the top 10 differentially expressed genes for each cluster.

(B–F) A Gene Ontology analysis for cluster 0 **(B)**, cluster 1 **(C)**, cluster 2 **(D)**, cluster 3 **(E)**, and cluster 4 **(F)**.

Supplementary Figure 8 (Hayashi et al.)

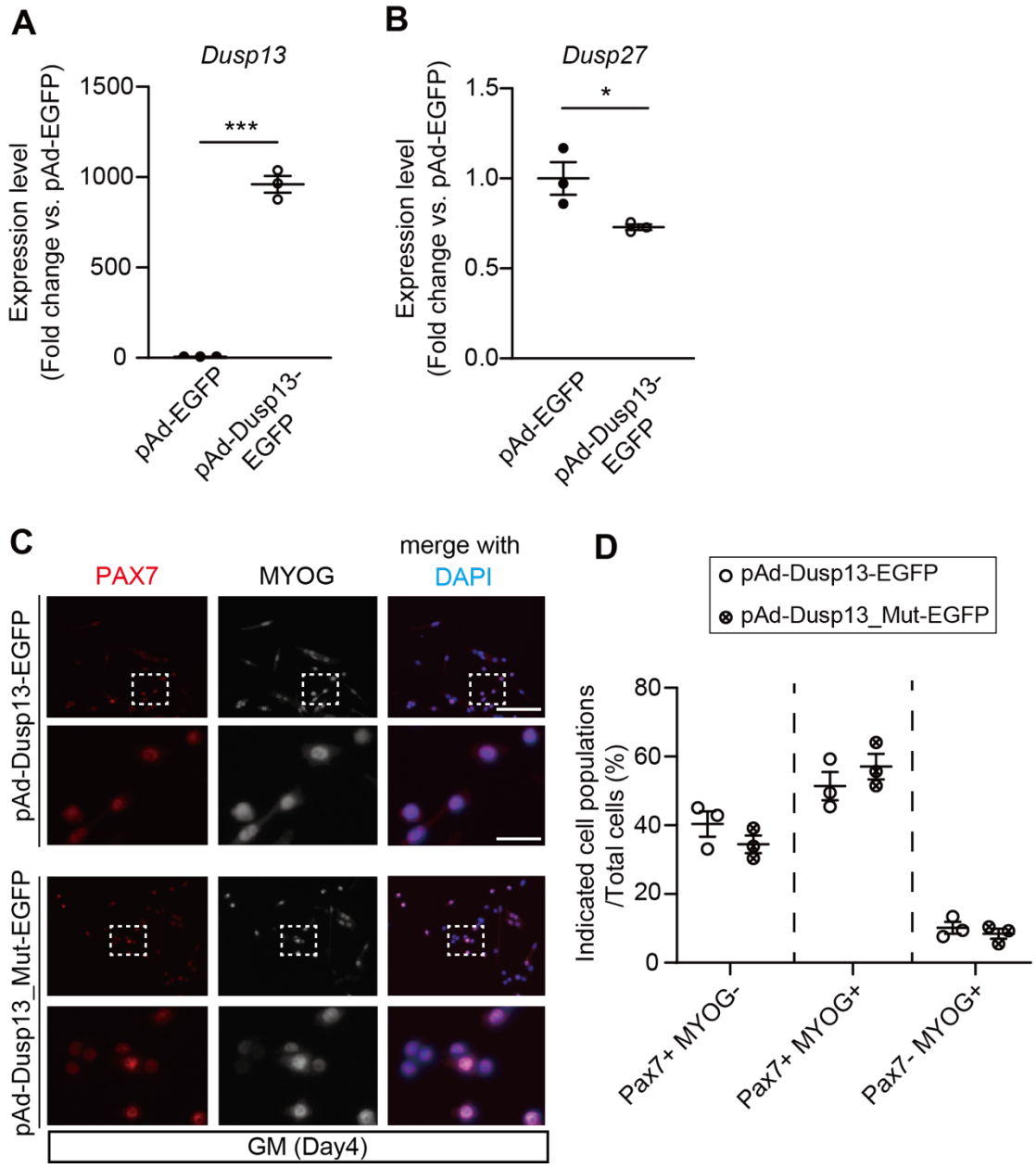

Figure S8. Expression levels of *Dusp13* and *Dusp27* in a *Dusp13* overexpression experiment.

(A, B) qPCR analysis of *Dusp13* **(A)** and *Dusp27* **(B)** mRNA levels in MuSCs which was overexpressed EGFP or *Dusp13*-EGFP (n = 3 per group).

(C) Immunofluorescence of PAX7 and MYOGENIN on cultured MuSCs after transduction with adenovirus vectors overexpressing Dusp13 (pAd-Dusp13-EGFP) or Dusp13 without phosphatase activity (pAd-DUSP13_Mut-EGFP). Nuclei are stained with DAPI (n = 3 per group).

(D) The proportion of each population in (**C**).

All data are represented as the mean ± standard error of the mean (SEM)

P values calculated using Student's t-test; *P < 0.05, ***P < 0.001.

Table S1. List of oligonucleotide sequences used as primers

Gene (genotyping)	Orientation	Sequence
Dusp13 (WT)	Fw	5′-GAATGAGGCTATTACCCGGC-3′
	Rv	5′-ACATAACCCACTCCTTCCGG-3′
Dusp13 (KO)	Fw	5′-CCCACATACATATTTGTAGGCACT-3′
	Rv	5′-GCCCCAATGCTAGGTTTACA-3′
Dusp27 (WT)	Fw	5′-AACCGAAAGCATCTTCATGG-3′
	Rv	5′-GTGGGCTAGAGAAGCATTCG-3′
Dusp27 (KO)	Fw	5′-TTGACCTGCCCTACATCTCC-3′
	Rv	5′-CTCACCCCAGGACAAGATGT-3′
Gene (RT-qPCR)	Orientation	Sequence
b-actin	Fw	5′-CATTGCTGACAGGATGCAGAAGG-3′
	Rv	5′-TGCTGGAAGGTGGACAGTGAGG-3′
Dusp13	Fw	5′-AAGTCTGGCCCAACCTTTTC-3′
	Rv	5′-CACTGCTGCCGTAGAAGTCA-3′
Dusp27	Fw	5′-AACCGAAAGCATCTTCATGG-3′
	Rv	5′-AGCCACGCTTTTCTCAGCTA-3′
Gene (Cloning)	Orientation	Sequence
Dusp13 for Adenovirus	Fw	5′-CCCAGGATCCATGTCACAGACC-3′
	Rv	5′-GGGTCTCGAGCTAGTGCTGCTGGCTC-3′
Dusp13 for Luciferase	Fw	5′-GCTCGCTAGCCTCGATAACCCTTGCAACAACTCC-3′
	Rv	5′-TCTTGATATCCTCGAACTTCATCCACTCTACTACA-3′
Dusp27 for Luciferase	Fw	5′-GCTCGCTAGCCTCGAATGTCTCCCACGAAGCCT-3′
	Rv	5′-TCTTGATATCCTCGAACACTCAGGGCAGACTGG-3′
MyoD	Fw	5′-GGATTCGCGAGAATTATGGAGCTTCTACGCCG-3′
	Rv	5′-CGACTCTAGAGAATTTCAAAGCACCTGATAAATCG-3′
Gene (Mutation)	Orientation	Sequence
Dusp13 D97A	Fw	5′-GACCCCTAGGGTCGGGTGCGGGAGGGA-3′
	Rv	5′-CTATAACTTTAGTCCCTCCCGCACCCG-3′
Dusp13 C128S	Fw	5′-CGATTCCACGACCACGTGAGGCACCAC-3′
	Rv	5′-AGCCGAGTGTGGGTGGTGCCTCACGTG-3′